

A Survey of Geometric Optimization for Deep Learning: From Euclidean Space to Riemannian Manifold

Yanhong Fei, Xian Wei, Yingjie Liu, Zhengyu Li, Mingsong Chen
Software Engineering Institute, East China Normal University

February 17, 2023

Abstract

Although Deep Learning (DL) has achieved success in complex Artificial Intelligence (AI) tasks, it suffers from various notorious problems (e.g., feature redundancy, and vanishing or exploding gradients), since updating parameters in Euclidean space cannot fully exploit the geometric structure of the solution space. As a promising alternative solution, Riemannian-based DL uses geometric optimization to update parameters on Riemannian manifolds and can leverage the underlying geometric information. Accordingly, this article presents a comprehensive survey of applying geometric optimization in DL. At first, this article introduces the basic procedure of the geometric optimization, including various geometric optimizers and some concepts of Riemannian manifold. Subsequently, this article investigates the application of geometric optimization in different DL networks in various AI tasks, e.g., convolution neural network, recurrent neural network, transfer learning, and optimal transport. Additionally, typical public toolboxes that implement optimization on manifold are also discussed. Finally, this article makes a performance comparison between different deep geometric optimization methods under image recognition scenarios.

1 Introduction

With increasing computing power, deep neural networks optimized in Euclidean space have achieved remarkable success from computer vision to natural language processing (e.g., autonomous driving and protein structure prediction) [1, 2]. However, to fully exploit the valuable information hidden in the data, most deep learning models tend to increase the capacity of their networks, either by widening the existing layers or by adding more layers [3, 4, 5]. For example, models often contain hundreds of convolution and pooling layers with various activation functions and multiple fully connected layers, producing millions or billions of parameters during training. These massive parameters associated with complex model architectures challenge the optimization of deep learning networks. As an alternative paradigm, optimization on the Riemannian manifold exploits hidden valuable information by utilizing geometric properties

of parameters, rather than increasing the network capacity. Therefore, geometric optimization can alleviate over-parameterization and feature redundancy problems. For example, deep learning models trained on the orthogonal manifold have less correlated parameters, making features much less redundant [6].

The optimization objective in most deep learning methods can be formulated as

$$\operatorname{argmin}_{\boldsymbol{\theta} \in \mathcal{D}} f_{\boldsymbol{\theta}}(\mathbf{x}), \text{ s.t. } C(\boldsymbol{\theta}), \quad (1)$$

where \mathcal{D} denotes the predefined admissible search space, f denotes a real-value optimization function (e.g., loss function) to be minimized by trainable parameters $\boldsymbol{\theta}$, and $C(\boldsymbol{\theta})$ represents constraints (e.g., orthogonality [6] and unit row sums [7]) that $\boldsymbol{\theta}$ is subject to. Most deep learning methods define the search space \mathcal{D} as the Euclidean space. However, parameters satisfying constraints are on the manifold, which is a low dimensional subspace and only occupies a small part of Euclidean space. Therefore, to eliminate constraints and reduce parameters, geometric optimization [8, 9, 10, 11] narrows the search space from Euclidean space to a smooth manifold. Hence, Equation (1) is transformed into a differentiable optimization function $f : \mathcal{M} \rightarrow \mathcal{R}$ on a Riemannian manifold, i.e.,

$$\operatorname{argmin}_{\boldsymbol{\theta} \in \mathcal{M}, \mathcal{M}=\{\boldsymbol{\theta} | C(\boldsymbol{\theta})\}} f_{\boldsymbol{\theta}}(\mathbf{x}). \quad (2)$$

As shown in Equation (2), selecting a manifold composed of points that meet constraints $C(\boldsymbol{\theta})$ in Equation (1), a large class of constrained deep learning problems in Euclidean space can be optimized as unconstrained and convex ones on the Riemannian manifold [10], which helps ensure the convergence. For example, a typical dimension reduction problem can be defined as follows

$$\operatorname{argmin}_{\boldsymbol{\theta} \in E} f_{\boldsymbol{\theta}}(\mathbf{x}) = -\operatorname{tr}(\boldsymbol{\theta}^T x^T x \boldsymbol{\theta}), \text{ s.t. } \boldsymbol{\theta}^T \boldsymbol{\theta} = I, \quad (3)$$

where E represents the Euclidean space, I represents the identity matrix and parameters $\boldsymbol{\theta}$ are constrained to be orthogonal. Since all matrices that satisfy orthogonality compose of the *Stiefel* manifold, Equation (3) can be treated as an unconstrained problem on the *Stiefel* manifold, which is a kind of Riemannian manifold.

Figure 1 depicts the intuitive paradigm for optimization processes in arbitrary Euclidean space and on Riemannian manifolds. Traditional optimization methods in Euclidean space may ignore the advantages of applying geometric optimization strategies. For example, the latter can obtain richer geometric information from different unique manifold structures and convert constrained optimization problems into unconstrained problems. Moreover, geometric optimization can achieve faster convergence speed and mitigate gradient explosion and disappearance problems in deep learning, which will be detailed in Section 4. Due to the above potential, geometric optimization has been applied to various deep neural networks in recent years, such as convolution neural network (CNN) [12, 6, 13], recurrent neural network (RNN) [14] and vision transformer (ViT) [15]. For instance, orthogonal parameterization is used in CNN to reduce filter similarities, make spectra uniform [16], and stabilize the activation distribution in different network layers [17]. However, there is a lack of comprehensive surveys focused

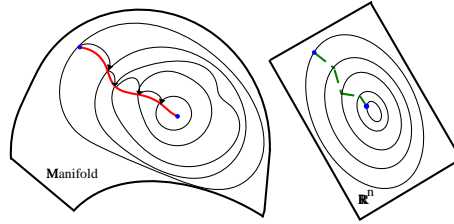


Figure 1: Comparison between geometric and Euclidean optimization path. The blue center point is the global optimum. The red curve describes the Riemannian optimization path converging upon the global optimal goal, always along a curve on manifolds. In contrast, the green dotted line indicates the Euclidean gradient descent path towards the optimal goal, taking the risk of moving off the manifold.

on deep learning methods applying geometric optimization. To explore benefits of geometric optimization, this article aims to give an overall review of recent advances on applying geometric optimization in deep learning.

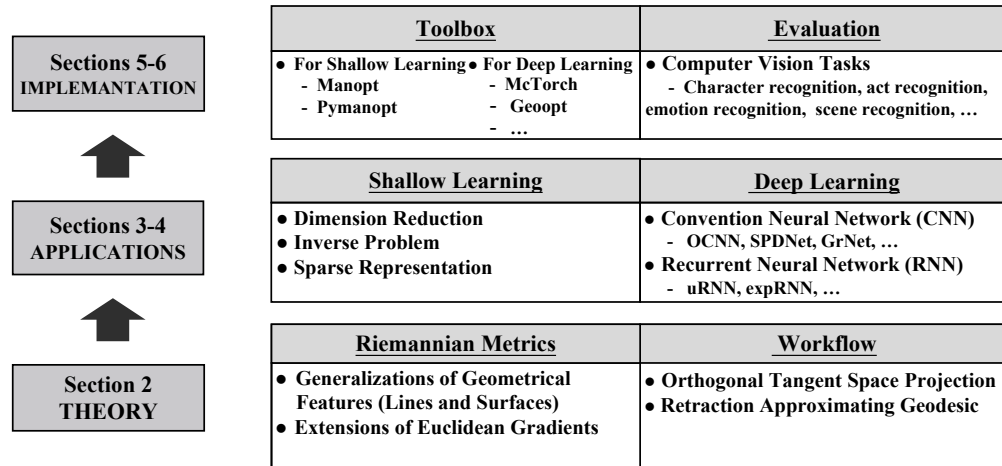


Figure 2: An overview of the central idea of this article.

¹ **Overview and article organization.** In this article, a survey of geometric optimization techniques for deep learning is presented, including the theory and applications of geometric optimization. Figure 2 displays an overview of the central idea of this article. Since the optimization theory is unified and model-independent, this article illustrates the theory first, including various geometric gradient descent optimizers

¹*Notations* In this work, vectors and matrices are denoted by bold lower case letters and upper case ones, respectively. Let \mathbb{R} be the set of real numbers, \mathbb{C} be the set of complex numbers and ∇f denotes the Euclidean gradient.

(Section 2). The motivation and technique of applying geometric optimization in classical machine learning is different from that of deep learning. Therefore, this article reviews how to apply geometric optimization to shallow learning (Section 3) and deep learning (Section 4) separately. In particular, this article investigates representative manifold optimization toolboxes (Section 5), followed by performance comparisons of different geometric deep learning methods on image recognition tasks (Section 6). Finally, we conclude the article and highlight future challenges and research trend (Section 7).

2 Geometric Optimization Theory

The essence of an optimization problem is to find the maximum or minimum value of a cost function. An unconstrained optimization problem can use conventional optimization methods (e.g., steepest descent method, conjugate gradient method, and Newton method) to find an optimal solution [18]. However, a broad range of optimization problems that occur in computer vision tasks are known as constrained optimization problems. In such a case, finding a closed form for the cost function is difficult. To use the aforementioned conventional optimization techniques, the constrained problem can be transformed into an unconstrained form by using the method of Lagrange multipliers or using a barrier penalty function [18]. However, the above methods hardly take advantage of underlying manifold structures. They merely treat the constrained problem as a “black box” and solve them by using algebraic manipulation.

As an alternative solution, geometric optimization methods are developed to exploit intrinsic geometric structures of objective function parameters. By utilizing the underlying geometry of a cost function, geometric optimization methods can narrow the search space of constrained optimization problems from Euclidean space to smooth Riemannian manifolds. Riemannian manifold has a differentiable structure and is equipped with smooth inner product and Riemannian gradients, which are different from Euclidean space and lay the foundation for geometric optimization. Based on the Riemannian inner product and Riemannian gradients, a broad spectrum of conventional optimization techniques in Euclidean space can have their counterparts on smooth manifolds [19, 20, 21, 8], including the steepest descent method [19, 20, 21], conjugate gradient descent method [22, 23, 24], trust-region method [8, 25] and Newton’s method [26, 8]. Therefore, geometric optimization methods can use Riemannian optimizers to find an optimal solution for objective functions.

In the following subsections, this article first illustrates the model-independent optimization process on the Riemannian manifold, covering basic concepts related to geometric optimization (Section 2.1). Next, this article briefly introduces various Riemannian gradient descent optimizers implementing geometric optimization, which is a counterpart of optimizers in Euclidean space (Section 2.2). Finally, this article presents a series of manifold structures that are commonly used in deep geometric learning methods (Section 2.3).

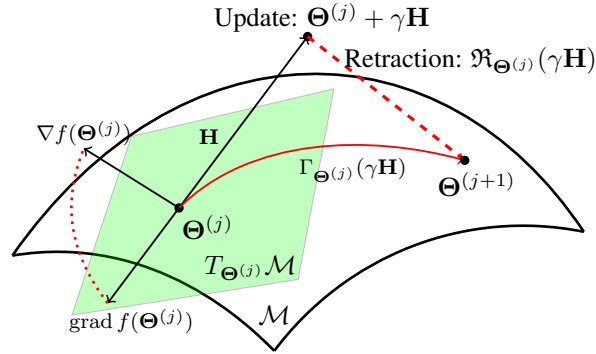


Figure 3: The update process in geometric gradient descent algorithm. It shows an update from the point $\Theta^{(j)}$ to the point $\Theta^{(j+1)}$ in a search direction $\mathbf{H} \in T_{\Theta^{(j)}}\mathcal{M}$ along the geodesic curve $\Gamma_{\Theta^{(j)}}(\gamma\mathbf{H})$. Moreover, it describes how to approximate the geodesic $\Gamma_{\Theta^{(j)}}(\gamma\mathbf{H})$ by using the retraction $\mathfrak{R}_{\Theta^{(j)}}(\gamma\mathbf{H})$.

2.1 Geometric Optimization Process on Manifolds

Figure 3 depicts the update process in geometric optimization[27] through the gradient descent example. There are two nearby points $\Theta^{(j)}$ and $\Theta^{(j+1)}$ on a manifold \mathcal{M} together with the tangent space at $\Theta^{(j)}$ (refer to the green area in Figure 3). Each point Θ on the manifold has its corresponding tangent space $T_{\Theta}\mathcal{M}$, which is a generalization of the tangent plane in Euclidean space and consists of all tangent vectors passing through Θ [28]. Each tangent space has an inner product, which is vital for vector metrics such as length and angles. Inner product space further helps induce the concept of orthogonality, an extension of vertical in higher dimensions. A Riemannian gradient $grad f(\Theta)$ for geometric optimization is a tangent vector on the tangent space $T_{\Theta}\mathcal{M}$ and points to the direction where the cost function on the manifold ascends steepest [28]. Figure 3 shows that gradient $\nabla f(\Theta)$ is computed in the ambient Euclidean space. Since the manifold is locally homomorphic to the Euclidean space, $grad f(\Theta)$ can be achieved by projecting Euclidean gradient $\nabla f(\Theta)$ to the appropriate tangent space $T_{\Theta}\mathcal{M}$, i.e.,

$$grad f(\Theta) = \Pi_{T_{\Theta}\mathcal{M}}(\nabla f(\Theta)), \quad (4)$$

where Π means the orthogonal projection.

As a counterpart of Euclidean straight lines, a geodesic is a locally shortest path between two points on the manifold. Therefore, reaching the optimal goal along a correct geodesic is shortest. Formally, a geodesic $\Gamma_{\Theta}(\gamma\mathbf{H})$ is a smooth curve on the manifold, proceeding from Θ in the direction of tangent vector $\mathbf{H} \in T_{\Theta}\mathcal{M}$ with a step size of $\gamma \in \mathbb{R}^+$ [23]. Since each tangent vector is the direction vector of a specific geodesic curve, it can uniquely determine a geodesic curve. In particular, the geodesic defined by the negative Riemannian gradient reveals the next point in the optimization direction. A point can be mapped from the tangent space to the manifold through exponential mapping. In practice, to alleviate the high computational cost of exponential

mapping, retraction operation $\mathfrak{R}_\Theta(\gamma\mathbf{H})$ is often used as an approximation [29]:

$$\mathfrak{R}_\Theta(\gamma\mathbf{H}) : T_p\mathcal{M} \rightarrow \mathcal{M}, \quad \gamma\mathbf{H} \rightarrow \Gamma_\Theta(\gamma\mathbf{H}), \quad (5)$$

where \mathbf{H} denotes an opposite vector of the Riemannian gradient. Therefore, \mathbf{H} points in the direction of the steepest descent of the optimization function. As a result, the optimization function will be minimized if parameter Θ is updated along a geodesic curve in the direction of \mathbf{H} . In summary, with a step size of γ , the optimizing process from the current parameter $\Theta^{(j)}$ to the next parameter $\Theta^{(j+1)}$ can be formulated as

$$\Theta^{(j+1)} = \Gamma_{\Theta^{(j)}}(\gamma\mathbf{H}) \approx \mathfrak{R}_{\Theta^{(j)}}(\gamma\mathbf{H}) = \mathfrak{R}_{\Theta^{(j)}}(-\gamma \text{grad} f(\Theta^{(j)})). \quad (6)$$

2.2 Gradient Descent Optimizers

Optimization problems defined in Euclidean space can be abstracted as

$$\min\{f_\theta(\mathbf{x}) : \theta \in \mathbb{E}\}, \quad (7)$$

where θ are trainable parameters and E means the Euclidean space. There are a variety of standard optimizers for Equation (7). The gradient descent method is a most basic optimization strategy. It can be improved by stochastic gradient descent (SGD), which can accelerate convergence. The other two typical variants of the gradient descent method are stochastic gradient descent-momentum (SGD-M) and root mean square prop (RMSProp). To solve valley oscillation and saddle point stagnation problems that SGD suffers from, SGD-M is developed to maintain the inertia of the previous step. According to empirical judgments of different parameters, RMSProp can adaptively determine the learning rate of parameters, i.e., parameters with low update frequency can have a larger learning rate, while parameters with high update frequency can reduce the step size. Let $\theta^{(k)}$ represent parameters at iteration k and $\theta^{(k+1)}$ represent parameters at iteration $k+1$, this section first explains the above Euclidean gradient descent optimizers and then shows how to generalize them to the Riemannian manifold for geometric optimization².

Gradient Descent. The gradient descent method takes the following form

$$\theta^{(k+1)} = \theta^{(k)} - \lambda \nabla f(\theta^{(k)}), \quad (8)$$

where λ is a hyper-parameter representing the step size. The negative direction of the gradient $\nabla f(\theta^{(k)})$ has a vital property, i.e., it is a descent direction of the optimization problem. Therefore, the optimization process is to iteratively update trainable parameters along the negative direction of gradient until convergence.

Stochastic Gradient Descent (SGD). The main idea behind SGD is to use random mini-batches of training data to update parameters of the optimization problem, which inherently reduces the calculation workload. Although the parameters may not be updated in the direction of the steepest descent every time, the overall update is in the steepest descent direction through multiple rounds of updates. As a result, SGD can greatly speed up the optimization process.

²For simplicity, this paper uses ∇f to denote $\frac{\partial f_\theta(x)}{\partial \theta}$ in Section 2.2.

Stochastic Gradient Descent-Momentum (SGD-M). Inspired by the concept of momentum in physics, SGD-M exerts the influence of the last update on the current update to damp oscillation and accelerate convergence. Let $m^{(k)}$ denote the update imposed on $\theta^{(k-1)}$ and ∇f denote the gradient at time k , the update $m^{(k+1)}$ to be imposed on $\theta^{(k)}$ can be achieved as

$$m^{(k+1)} = \lambda_0 m^{(k)} + \lambda_1 \nabla f, \quad (9)$$

where λ_0 and λ_1 are hyper-parameters. Sequentially, the parameter $\theta^{(k)}$ is updated to $\theta^{(k+1)}$ by $m^{(k+1)}$ as follows

$$\theta^{(k+1)} = \theta^{(k)} - m^{(k+1)}. \quad (10)$$

Root Mean Square Prop (RMSProp). Similar to SGD-M, RMSProp considers the influence of the last update when calculating the upcoming update. Let $m^{(k)}$ be the update on the previous occasion and ∇f be the current gradient, RMSProp designs upcoming update $m^{(k+1)}$ as follows

$$m^{(k+1)} = \lambda m^{(k)} + (1 - \lambda)(\nabla f \odot \nabla f), \quad (11)$$

where λ is a hyper-parameter and \odot denotes the *Hadamard* product [29] which is element-wise. RMSProp updates $\theta^{(k)}$ to $\theta^{(k+1)}$ in the following way, i.e.,

$$\theta^{(k+1)} = \theta^{(k)} - \eta \frac{\nabla f}{\sqrt{m^{(k+1)} + \epsilon}}, \quad (12)$$

where η is a hyper-parameter and ϵ is positive to prevent the denominator from being zero. Using element-wise square root and division operation, RMSProp guarantees that different elements in gradient ∇f have different coefficients, which represent learning rates in deep learning. Therefore, RMSProp enables parameters to have different learning rates [29], which makes the optimization process more flexible.

Based on the aforementioned optimization process on manifolds (Section 2.1), the Euclidean gradient descent algorithm in Equation (8) can be transferred to Riemannian manifolds as

$$\theta^{(k+1)} = \mathfrak{R}_{\theta^{(k)}}(-\lambda \text{grad} f(\theta^{(k)})), \quad (13)$$

where $\mathfrak{R}_{\theta^{(k)}}$ means the retraction operation at point $\theta^{(k)}$ and $\text{grad} f$ means the Riemannian gradient. For better understanding, this article takes constraint SGD-M and constraint RMSProp as an instance to explain how to generalize gradient descent optimizers from Euclidean space to manifolds. By performing orthogonal projection and retraction, other Euclidean gradient descent optimizers can be similarly converted to Riemannian optimizers.

Constraint SGD-M [29]. Constraint SGD-M is a generalization of SGD-M optimizer on manifolds. In the k -th iteration, $m^{(k)}$ denotes a tangent vector on the tangent space $T_{\theta^{(k-1)}}M$ and $m^{(k+1)}$ denotes another vector on the tangent space $T_{\theta^{(k)}}M$. Since ∇f is in the surrounding Euclidean space, it needs to be orthogonally projected to tangent space $T_{\theta^{(k)}}M$, i.e., the current Riemannian gradient $\text{grad} f$ is achieved as follows

$$\text{grad} f = \Pi_{T_{\theta^{(k)}}M}(\nabla f). \quad (14)$$

The transportation from a tangent space associated with point p to another tangent space associated with point q is called parallel transportation, i.e., $\Gamma_{p \rightarrow q} : T_p M \rightarrow T_q M$. After projecting the Euclidean gradient ∇f to the tangent space $T_{\theta^{(k)}} M$ and transporting $m^{(k)}$ from $T_{\theta^{(k-1)}} M$ to $T_{\theta^{(k)}} M$, Equation (9) is transformed to:

$$m^{(k+1)} = \lambda_0 \Gamma_{\theta^{(k-1)} \rightarrow \theta^{(k)}}(m^{(k)}) + \lambda_1 \Pi_{T_{\theta^{(k)}} M}(\nabla f). \quad (15)$$

Based on the retraction operation, the optimization parameter $\theta^{(k+1)}$ can be updated from $\theta^{(k)}$ by searching along the geodesic in the negative direction of $m^{(k+1)}$, i.e., the iterate optimization can be expressed as

$$\theta^{(k+1)} = \mathfrak{R}_{\theta^{(k)}}(-m^{(k+1)}). \quad (16)$$

Constraint RMSProp [29]. Similar to constraint SGD-M, after transporting $m^{(k)}$ from tangent space $T_{\theta^{(k-1)}} M$ to $T_{\theta^{(k)}} M$ and orthogonally projecting $\nabla f \odot \nabla f$ to corresponding tangent space, Equation (11) can be transformed into:

$$m^{(k+1)} = \lambda \Gamma_{\theta^{(k-1)} \rightarrow \theta^{(k)}}(m^{(k)}) + (1 - \lambda) \Pi_{T_{\theta^{(k)}} M}(\nabla f \odot \nabla f). \quad (17)$$

The parameter $\theta^{(k+1)}$ of the optimization goal can be iteratively searched on the manifold with a determined direction $-\eta \frac{\Pi_{T_{\theta^{(k)}} M}(\nabla f)}{\sqrt{m^{(k+1)} + \epsilon}}$, that is,

$$\theta^{(k+1)} = \mathfrak{R}_{\theta^{(k)}}\left(-\eta \frac{\Pi_{T_{\theta^{(k)}} M}(\nabla f)}{\sqrt{m^{(k+1)} + \epsilon}}\right). \quad (18)$$

2.3 Manifold Examples

Different kinds of matrix manifolds have different geometry structures and satisfy different constraints, bringing different advantages when applying geometric optimization to deep learning. For example, the oblique manifold plays a significant role in dictionary learning due to its property of unit-norm columns, while the *Stiefel* manifold has a positive effect on optimizing RNNs since matrices on the *Stiefel* manifold have orthogonal and uncorrelated columns, which helps alleviate feature abundance problems in RNNs. Since space is limited, this section only presents common manifold structures³ such as *Stiefel* manifold, oblique manifold, and *Graßmann* manifold, all of which are widely used in existing geometric optimization techniques that are discussed in Section 3 and Section 4.

Product Manifold and Quotient Manifold. Let \mathcal{A} and \mathcal{B} be two manifolds of dimension d_A and d_B , for any pair of charts (U, ϕ) and (V, φ) of \mathcal{A} and \mathcal{B} , the map Φ is defined on $U \times V$ by $\Phi(x, y) = (\phi(x), \varphi(y))$. It specifies a smooth product manifold structure on the product space $\mathcal{A} \times \mathcal{B}$. Quotient manifold is an abstract space with similar subsets in the same manifold. These subsets can be described with equivalence relationship. \mathcal{A} represents a manifold equipped with an equivalence relation

³For more introduction on matrix manifolds, we refer interested readers to the website <https://www.Pymanopt.org>.

\sim , which satisfies three properties, i.e., reflexivity, symmetry and transitivity [8]. The equivalence class of one point x consists of all elements that are equivalent to it, i.e.,

$$[x] := \{y \in \mathcal{A} : y \sim x\}, \quad (19)$$

where $[x]$ indicates the equivalence class of x . The quotient of manifold \mathcal{A} by relation \sim is defined as follows

$$\mathcal{A}/\sim := \{[x] : x \in \mathcal{A}\}, \quad (20)$$

with the projection $\pi : \mathcal{A} \rightarrow \mathcal{A}/\sim$, indicated by $x \rightarrow [x]$. When π is a submersion projection, and \mathcal{A} is a smooth manifold [8, 30], \mathcal{A}/\sim admits a unique smooth manifold structure B , which is the quotient manifold of \mathcal{A} .

Symmetric Positive-Definite Manifold [29]. It consists of Symmetric Positive-Definite (SPD) matrices $M \in \mathbb{R}^{p \times p}$ equipped with the Affine Invariant Riemannian Metric (*AIRM*) as follows

$$S_{++}^p \triangleq \{M \in \mathbb{R}^{p \times p} : v^T M v > 0, \forall v \in \mathbb{R}^p - \{0_p\}\}. \quad (21)$$

SPD manifold achieves great success in computer vision due to its powerful statistical representations for images and videos. For example, SPD matrices are used to construct region covariance matrices for pedestrian detection [31], joint covariance descriptors for action recognition [32], and image set covariance matrices for face recognition [33].

Stiefel Manifold [29]. The *Stiefel* manifold $St(p, n)$ is composed of orthogonal matrices $W \in \mathbb{R}^{n \times p}$ ($p \leq n$) endowed with the Frobenius inner product as follows

$$St(p, n) \triangleq \{W \in \mathbb{R}^{n \times p} : W^T W = I_p\}, \quad (22)$$

where I_p denotes $\mathbb{R}^{p \times p}$ identity matrix. The optimization function over the compact *Stiefel* manifolds has an upper bound, which allows it to achieve an optimal solution.

Sphere Manifold and Oblique Manifold. The set of unit Frobenius norm matrices of size $n \times m$ is denoted by the sphere \mathbb{S}^{nm-1} . It can be treated as a Riemannian submanifold embedded in Euclidean space $\mathbb{R}^{n \times m}$ endowed with the usual inner product $\langle H_1, H_2 \rangle = \text{trace}(H_1^T H_2)$. The oblique manifold $\mathcal{OB}(n, m)$ is the set of matrices of size $n \times m$ with unit-norm columns. It has the same geometry as that of the product manifold of spheres $\prod_{i=0}^m \mathbb{S}^{n-1}$.

Graßmann Manifold [29]. The *Graßmann* manifold $\mathcal{G}(n, p)$ embraces the set of subspaces spanned by the orthogonal matrices $X \in \mathbb{R}^{n \times p}$ ($p \leq n$) as

$$\mathcal{G}(n, p) \triangleq \{\text{Span}(X) : X \in \mathbb{R}^{n \times p}, X^T X = I_p\}. \quad (23)$$

Note that a *Graßmann* manifold is different from a *Stiefel* manifold, i.e., a point on the *Stiefel* manifold represents a basis for a subspace, whereas a point on the *Graßmann* manifold represents an entire subspace. Moreover, *Graßmann* manifolds are of linear subspaces and can be used to perform a geometry-aware dimension reduction.

Unitary Manifold. Unitary matrices are the extension of orthogonal matrices to the complex domain, i.e.,

$$U(n) \triangleq \{U \in \mathbb{C}^{n \times n} : U^* U = I_n\}, \quad (24)$$

where U^* denotes the conjugate transpose matrix and I_n represents the identity matrix of size $n \times n$. Orthogonal or unitary matrices can preserve norm of vectors, i.e., $\|Wh\|_2 = \|h\|_2$ when W is an orthogonal or unitary matrix. Therefore, exploding and vanishing gradient problems in deep temporal networks can be alleviated when parameters are optimized on the orthogonal or unitary manifold, which will be detailed in Section 4.2.

Lie Group [13]. Lie groups are real or complex manifolds with group structure. There are two compact and connected Lie groups, i.e., the special orthogonal group formulated as

$$SO(n) = \{B \in \mathbb{R}^{n \times n} | B^T B = I, \det(B) = 1\}, \quad (25)$$

and the unitary group formulated as

$$U(n) = \{B \in \mathbb{C}^{n \times n} | B^* B = I\}. \quad (26)$$

The tangent space at the identity element of the Lie group is called the *Lie algebra* of it. For the special orthogonal group and the unitary group, their Lie algebras are given by

$$\begin{aligned} \mathfrak{so}(n) &= \{A \in \mathbb{R}^{n \times n} | A + A^T = 0\}, \\ \mathfrak{u}(n) &= \{A \in \mathbb{C}^{n \times n} | A + A^* = 0\}. \end{aligned} \quad (27)$$

$\mathfrak{so}(n)$ is known as skew-symmetric matrix, while $\mathfrak{u}(n)$ is skew-Hermitian matrix. The Lie exponential map ($exp : \mathfrak{g} \rightarrow G$ where G denotes the Lie Group and \mathfrak{g} denotes its Lie algebra) on a connected, compact Lie group is surjective. Therefore, the optimization problem on a Lie group can be converted to the optimization problem in Euclidean space where Euclidean gradient descent optimizers can be directly used.

3 Applications in Classical Machine Learning

Classical machine learning methods gained achievements in solving artificial intelligence problems (e.g., dimension reduction, inverse problem, sparse representation, analysis operator learning, and temporal models). Despite the increasing computing power of modern computer facilities, it is still difficult to solve a large category of constrained classical machine learning problems in Euclidean space. To decrease the solving difficulty, geometric optimization focuses on the special structure of constrained problems and regards them as unconstrained ones on Riemannian manifolds [10].

3.1 Dimension Reduction

By using a mapping $\mu: \mathbb{R}^m \rightarrow \mathbb{R}^l$ with $l < m$, dimension reduction (DR) aims to find a lower-dimensional representation $y_i \in \mathbb{R}^l$ of given data samples $x_i \in \mathbb{R}^m$. The most popular DR paradigm uses a linear projection while others employ a nonlinear transformation to constrain locality properties between data. Table 1 summarizes main properties of mainstream DR approaches (e.g., linear discriminant analysis (LDA) [34], principal component analysis (PCA) [35, 36, 37], multi-dimensional scaling (MDS) [38, 39], isometric feature mapping (ISOMAP) [40], local linear embedding (LLE) [41], laplace eigenmaps (LE) [42], and locality preserving projections (LPP) [43]).

The mapping $\mu: \mathbb{R}^m \rightarrow \mathbb{R}^l$ used in DR methods is often restricted to be an orthogonal projection, i.e.,

$$\mu(\mathbf{x}) := \mathbf{V}^\top \mathbf{x}, \quad (28)$$

where the orthogonal matrix $\mathbf{V} \in \mathbb{R}^{m \times l}$ belongs to the *Stiefel* manifold $St(l, m) := \{\mathbf{V} \in \mathbb{R}^{m \times l} | \mathbf{V}^\top \mathbf{V} = \mathbf{I}_l\}$. One generic algorithmic framework to find an optimal $\mathbf{V} \in St(l, m)$ can be formulated as a maximization problem, i.e.,

$$\operatorname{argmax}_{\mathbf{V} \in St(l, m)} \frac{\operatorname{tr}(\mathbf{V}^\top \mathbf{A} \mathbf{V})}{\operatorname{tr}(\mathbf{V}^\top \mathbf{B} \mathbf{V}) + \sigma}, \quad (29)$$

where matrices $A, B \in \mathbb{R}^{m \times m}$ are often symmetric or positive definite matrices. Equation (29) is called *trace quotient* or *trace ratio*. Note that constant $\sigma > 0$ can prevent the denominator from being zero. Matrices A and B are constructed to measure the similarity between data points according to specific problems. V is not unique and closely related to selected eigenvalues. Solutions of Equation (29) are rotation invariant, i.e., let $\mathbf{V}^* \in St(l, m)$ be a solution of the problem, then $\mathbf{V}^* \Theta$ for any orthogonal $\Theta \in \mathbb{R}^{l \times l}$ is also a solution of Equation (29). In other words, the solution set of Equation (29) is the set of all l -dimensional linear subspaces in \mathbb{R}^m , which can be represented by *Grassmann* manifold, i.e.,

$$\mathfrak{G}r(l, m) := \{\mathbf{V} \mathbf{V}^\top | \mathbf{V} \in St(l, m)\}. \quad (30)$$

As shown above, most linear DR methods begin with solving $tr(V^T AV)$ while non-linear DR methods construct a graph by connecting nearby points, which captures information on the local neighborhood structure of data and forms a similar optimization problem. Taking the non-linear DR method LE as an example, the Laplace matrix associated with the neighborhood graph [44] can be regarded as the symmetric matrix A in Equation (29).

3.2 Inverse Problem

Aiming to explore internal patterns from phenomena [45], an inverse problem has a significant impact on practical applications. For example, the following practical problems can be modeled as inverse problems: i) deducing structural information in human body from the X-ray; and ii) inferring interior appearance of stratigraphy from seismic wave. An inverse problem can be viewed as reconstructing inputs from outputs as follows,

$$\mathbf{y} = \mathbf{W} \mathbf{x}, \quad (31)$$

where $\mathbf{y} \in \mathbb{R}^l$ is the given output and \mathbf{W} is a matrix that maps input data \mathbf{x} to output data \mathbf{y} . The goal of the inverse problem in Equation (31) is to recover \mathbf{x} on the premise that \mathbf{y} is a priori. It is challenging to get a precise solution, however, an approximate solution can be achieved by confining the parameter matrix \mathbf{W} to reside on a smooth Riemannian manifold. Let the sum of elements in the same row of matrix \mathbf{W} be exact 1, Equation (31) can be solved by optimization on the oblique manifold \mathcal{M} where matrices all have unit row sums [7], i.e.,

$$\min_{\mathbf{W} \in \mathcal{M}} \|\mathbf{y} - \mathbf{W} \mathbf{x}\|_2^2. \quad (32)$$

Table 1: Summary of Dimension Reduction Algorithms

Methods	Linear/Non-Linear ¹	Global/Local ²	Properties
LDA	Linear	Global	is supervised, uses prior knowledge of categories, is limited to Gaussian distribution samples
PCA	Linear	Global	is unsupervised, uses orthogonal principal components to eliminate interactions between each components
MDS	Non-Linear	Global	has simple calculation, preserves the data relationship in original space, is visualization-friendly, mistakenly assumes that each dimension has a same contribution
ISOMAP	Non-Linear	Global	suits low dimensional manifolds with a flat interior rather than that with large internal curvature, has high computation cost
LLE	Non-Linear	Local	suits non-closed locally linear low dimensional manifolds, has small computational complexity, is limited to dense uniform dataset, is sensitive to the number of nearest neighbor samples
LE	Non-Linear	Local	preserves local features, is less sensitive to outliers and noise, has a stable embedding
LPP	Linear	Local	is defined at any point in space, i.e., can be generalized to the testing set and not limited to the training set

¹ Linear represents linear projection mapping, while non-linear represents non-linear projection mapping.

² The global/local represents the geometric relationship of the input data.

3.3 Dictionary Learning

As a specific inverse problem, dictionary learning has been widely used to obtain the most essential features of input data [23]. Let $X \in R_{n \times k}$ denote the input sample, in dictionary learning, X is expanded into a linear combination as

$$X = D_1\phi_1 + \dots + D_n\phi_n, \quad (33)$$

where D_1, \dots, D_n represent the most essential features to be learned from the input, while ϕ_1, \dots, ϕ_n indicate combination coefficients of features D_1, \dots, D_n . Let $D \in R_{k \times n}$ indicate the dictionary set $\{D_1, \dots, D_n\}$ and $\Phi \in R_{n \times r}$ indicate the set $\{\phi_1, \dots, \phi_n\}$, Equation (33) can be simplified as follows,

$$X = D\Phi, \quad (34)$$

where D and Φ can have various kinds of combinations. Dictionary learning aims to learn a D that makes the coefficients Φ be zero or close to zero, i.e., a sparse representation of samples X . The dictionary D and the sparse coefficients Φ are calculated alternately. When Φ is fixed, the dictionary learning part is the same as the form of Equation (31), which is an inverse problem of reconstructing D . Let $\|\phi\|_0$ denote the number of entries in Φ that are different from zero, the dictionary D is subject to $\|D_1\| = \dots = \|D_n\| = 1$. Therefore, the above dictionary learning problem can be transformed to the following minimization problem on the oblique manifold:

$$\operatorname{argmin}_{D \in OB(k,n)} \|X - D\Phi\|_2^2 + \lambda \|\Phi\|_0. \quad (35)$$

3.4 Analysis Operator Learning

Analysis operator learning assumes that a few operators are sufficient to represent observed high-dimensional variables [46]. However, these operators are implicit and

unobserved, for instance, store environment and service quality are latent operators hidden behind the observed variable “price”. The goal of analysis operator learning is to find out these invisible operators, since low-dimensional operators can simplify original high-dimensional variables.

Let X be original high-dimensional variables and F be latent operators with lower dimensions, the analysis operator learning can be generally formulated as follows

$$X = AF, \quad (36)$$

where A denotes the operator loading matrix, in which the element A_{ij} represents the load of variable x_i on factor f_j . It is proved that the parameter A can be positive [47], the analysis operator learning can therefore be converted to an optimization problem on the positive manifold \mathcal{M} as follows

$$\min_{A \in \mathcal{M}} \|X - AF\|_2^2. \quad (37)$$

3.5 Temporal Model

The temporal probability model is composed of a transition model describing the state evolution over time and a sensor model describing the observation process [27]. A temporal model is helpful to cope with filtering, prediction and smoothing. In the transition model, next state z_{t+1} is transitioned from the current state z_t , independent from previous states. Given the time-relevant transition probability $A(t)$, the transition process of states can be modeled as

$$z_{t+1} = A(t) \cdot z_t + \epsilon(t), \quad (38)$$

where the noise $\epsilon(t)$ follows the Gaussian distribution.

States are invisible and a hidden state can manifest as a specific observation with the help of an emission probability. The current observation x_t is only defined by the current state z_t , having nothing to do with previous states and observations. Given a time-varying emission probability $C(t)$, the observation process can be modeled as

$$x_t = C(t) \cdot z_t + \delta(t), \quad (39)$$

where the noise $\delta(t)$ follows the Gaussian distribution.

As a mixture of Equation (38) and Equation (39), temporal models can be divided into hidden Markov models and linear dynamic systems. A hidden Markov model has discrete hidden state variables while the hidden state and observed variables of a linear dynamic system obey Gaussian distribution. Let n represent the size of the temporal sequence, the expectation of observation sequences $E[x_0, x_1, x_2 \dots]$ can be deduced as:

$$[C(t), C(t)A(t), C(t)A(t)^2 \dots C(t)A(t)^{n-1}] z_0, \quad (40)$$

where z_0 is the initial hidden state. It can be considered as a sequence of subspaces spanned by the emission and transition matrix columns at the corresponding time [48]. As is mentioned in Section 2.3, a point on the *Graßmann* manifold is a subspace. Therefore, the temporal model can be mathematically optimized on the *Graßmann* manifold.

4 Applications in Deep Learning

With the increasing attention to geometric optimization, more and more deep learning methods have developed to combine with it. Geometric optimization techniques vary with different deep learning backbones (e.g., CNN, RNN and GNN). Therefore, this section classifies applications in deep learning into the following categories, i.e., i) geometric CNN; ii) geometric RNN; iii) geometric GNN and iv) geometric optimization for other deep learning methods, such as transfer learning and optimal transport. Orthogonal manifold is widely employed in geometric CNNs to reduce feature redundancy. Examples include utilizing kernel orthogonality in Orthogonal CNNs [6], optimization on Submanifolds of Convolution Kernels in CNNs [49], and regularizing the convolution kernel with orthogonality when training deep CNNs [12]. In addition, geometric CNNs can leverage the unique structure of *Stiefel* manifold [50] and *Graßmann* manifold [51]. Geometric RNNs take advantage of the norm-keeping property of orthogonal and unitary manifolds to alleviate gradient explosion and vanishing problems. Examples include complex unitary matrices in Unitary Evolution Recurrent Neural Networks [14], and the special orthogonal group and unitary group in Cheap Orthogonal Constraints: A Simple Parameterization of the Orthogonal and Unitary Group [13]. Geometric GNNs pay much attention to hyperbolic manifold and extensively use it for structure capturing. Examples include the hyperbolic GNN [52] and a geometric neural network which incorporates Euclidean space with hyperbolic geometry [53].

4.1 Geometric CNN

Deep CNN has achieved great success in various computer vision tasks, such as image recognition [54] and segmentation tasks [55]. CNN can automatically learn features from large-scale data by benefiting from three essential structures, i.e., convolution, activation, and pooling structures [10]. Although CNNs have worked efficiently, using the entire Euclidean space to search optimal solutions cause problems (e.g., training instability and feature redundancy) that hinder the further development. To alleviate these problems, geometric optimization approaches optimize CNNs on the suitable Riemannian manifold via kernel space, geometric regularization, and quasi-CNN architectures with parameters on the manifold.

Kernel Space. A low-dimensional manifold is often embedded in the high-dimensional Euclidean space. Kernel functions can map original features to a higher dimensional space. Therefore, with the help of kernel functions, computationally cheap operations on manifolds can represent complex operations in Euclidean space. Kernel spaces can be utilized and described by topological smooth manifolds. For example, positive-definite kernels, which are known as *Graßmann* kernels on the *Graßmann* manifold, can be used to map the manifold into a Hilbert space [56]. Zhang et al. [57] designed a new kind of *Graßmann* kernel based on canonical correlations to distinguish one class from others more accurately. Liu et al. [58] designed RBF kernels for linear subspace, covariance matrix, and Gaussian distribution to optimize emotion video recognition on the Riemannian manifolds. Hariri et al. [59] defined a kernel based on the SPD covariance matrix to indicate the similarity of two face images for face matching.

Kernel space constructed on nonlinear data helps learn the inherent manifold struc-

ture. Yuan et al. [60] combined manifold kernel space with deep learning architecture for scene recognition. To preserve the geometric structure of input scene images and achieve a greater representational ability, [60] defines a low-level feature layer X and a hidden manifold kernel space Y as a base unit. Moreover, the deep architecture is unit-by-unit and Y_k serves as the input of another base unit to generate the next hidden space Y_{k+1} . Comparative experiments evaluate the performance of the manifold regularized deep network on the large-scale scene data set.

Ozay et al. [49] considered the kernel estimation problem in CNNs as an optimization on embedded or immersed submanifolds of kernels. [49] explores geometric properties of convolution kernel space in CNNs and reveals that different kernel normalization methods induce different geometric properties. For example, the orthonormal normalization manner implies *Stiefel* manifold, while kernels normalized with the unit-norm reside on the sphere manifold. Furthermore, [49] proposes an SGD algorithm for optimization on kernel submanifolds. Experiments carried out on three kernel submanifolds confirm that the above approach can boost the performance of traditional CNN training.

Geometric Regularization. Regularization acts as the penalty term of the optimization function. It is used to impose restrictions on the parameters of the optimization function. The commonly used geometric regularization is the orthogonal constraint, aiming to restrict parameters to be on the orthogonal manifold. Recall orthogonal matrices $W^T W = I$ introduced in Section 2.3, orthogonal regularization methods are roughly divided into hard orthogonality as

$$\|W^T W - I\|_F^2 \quad (41)$$

and soft orthogonality as

$$\lambda \|W^T W - I\|_F^2 \quad (42)$$

where $\|\cdot\|_F$ indicates the Frobenius norm and λ represents a relaxation coefficient. Based on the soft orthogonality, we can achieve double soft orthogonality as

$$\lambda(\|W^T W - I\|_F^2 + \|W W^T - I\|_F^2). \quad (43)$$

Based on the observation that the kernel orthogonality is necessary but insufficient for the orthogonal convolution, Wang et al. [6] proposed an approach where orthogonality constraints directly regularize a convolution layer. During training, the convolution filter K is transformed into a Doubly Block-Toeplitz (DBT) matrix and the spectrum is regularized to be uniform, which requires row or column orthogonality. The orthogonality constraint on the DBT matrix helps relieve exploding and vanishing gradient problems, making the training more stable. Moreover, a number of experiments show that it can achieve amazing performance such as stronger robustness and better generalization.

Bansal et al. [12] observed that orthogonality can stabilize the energy distribution of activations within CNNs and enhance the efficiency of training. [12] compares different orthogonality regularizers, e.g. soft orthogonality, double soft orthogonality and mutual coherence regularization that lowers the column correlation as much as possible to enforce orthogonality. Meanwhile, [12] designs a novel orthogonality regularizer

named Spectral Restricted Isometry Property Regularization, which focuses on minimizing the spectral norm of $W^T W - I$. Remarkable experimental results suggest that regarding orthogonality regularizations as standard tools for training deep CNNs offers better accuracy and stability.

In order to estimate human face poses under challenging circumstances such as complex background or various orientations, Hong et al. [61] proposed manifold regularized convolutional layers (MRCL) to enhance the nonlinear locality constraints of CNN parameters. With MRCL being on top of traditional CNN’s pooling and activation operations, a low-rank manifold structure of latent data can be recovered for better optimization. By employing multitask learning with low-rank learning, multimodal of different data representations can be combined to predicate face postures. Comparative experiments validate the benefit of imposing manifold regularization to traditional convolutional layers.

Roufousse et al. [62] proposed a spectral unsupervised functional map network (SURFMNet) where the matching network from one shape to another is constrained to the orthogonal manifold. SURFMNet computes correspondences across 3D shapes using unsupervised learning, i.e., building shape correspondences without ground truth. Solid experimental results support the consistent superiority of SURFMNet compared to state-of-the-art unsupervised shape matching methods. Experimental results also show that SURFMNet is comparable to supervised ones.

Different from existing methods that shallowly learn Lie group features, Huang et al. [63] incorporated a Lie group structure to parameter matrices in the deep human action recognition network. The proposed skeleton-based human model (V, E) is a binary relation, where V represents a set of vertexes that consists of body joints (v_1, \dots, v_N) and E represents a set of edges that consists of body bones (e_1, \dots, e_M) . The rotation matrix is represented by the axis-angle model based on the skeleton and forms the special orthogonal group. To preserve the Lie group structure of the input rotation matrix, the above human action recognition network is optimized on the Lie group manifold and mapped to a tangent space for the final classification.

Similar to the above action recognition network [63], Chen et al. [64] put forward a deep manifold learning (DML) framework to learn manifold information and deep representations of action videos. [64] studies that leveraging geometry information in deep learning contributes to high accuracy and efficiency for action recognition. To extract more expressing features, the DML framework applies a manifold regularizer on the previous layer, label information and manifold parameters. Furthermore, adapting the DML framework to restricted Boltzmann machine can relieve the overfitting problem and improve the recognition accuracy.

Quasi-CNN Architecture. Kernel methods and orthogonal regularization do not change fundamental CNN components (e.g., convolution and pooling operations). Another method of applying geometric optimization to deep learning is to mimic traditional CNN architecture and establish a new architecture suitable for the manifold structure. In this article, the above architecture is named as quasi-CNN architecture. Convolution and activation layers are rebuilt to induce geometric optimization in the quasi-CNN architecture. To achieve this goal, parameters in the quasi-CNN architecture are designed to reside on the compact *Stiefel* manifold. For a more intuitive explanation, this article takes the deep SPD matrix network (SPDNet) [50] and deep

Graßmann neural network architecture (GrNet) [51] as examples.

Let X be the input, and W be the transformation parameter on the compact *Stiefel* manifold. First, SPDNet is designed for optimization on the SPD manifold. Bilinear mapping (BiMap) layer $f_b = WXW^T$ plays the role of convolution layers in traditional CNNs. Based on the eigenvalue decomposition $X = U\Sigma U$, eigenvalue rectification (ReEig) layers $f_r = U\max(\epsilon I, \Sigma)U^T$ are designed to replace nonlinear activation layers and ϵ is the activation threshold. SPDNet designs the eigenvalue logarithm (LogEig) layer to flatten the Riemannian manifold to a flat space where classical Euclidean computations can be applied. GrNet is designed for optimization along the orthonormal manifold. Full rank mapping (FRMap) layers $f_{fr} = WX$ in GrNet replace the convolution layer in traditional CNNs. Inspired by the QR decomposition $X = QR$ where Q is orthonormal, GrNet designs re-orthonormalization (ReOrth) layer $f_{fo} = XR^{-1} = Q$ to achieve an orthonormal output. Unlike the LogEig layer in SPDnet, GrNet uses inner product XX^T to reduce the manifold to a flat Euclidean space. After pooling operations on the resulting Euclidean data, GrNet designs orthonormal mapping (OrthMap) layer $f_{om} = U_{1:q}$ to transform the output matrix back to the orthonormal manifold, where $U_{1:q}$ denotes the first q largest eigenvectors achieved by the eigenvalue decomposition.

4.2 Geometric RNN

RNNs are designed to process sequential data since they can capture spatial and temporal dependencies between the sequential input. Therefore, RNN can be applied in tasks such as speech recognition, text prediction, and machine translation. Given an input sequence $X_\tau = x_1, x_2, \dots, x_\tau$ ($x_i \in \mathbb{R}^n$) with length τ , a basic RNN framework is aimed to generate the output sequence $Y_\tau = y_1, y_2, \dots, y_\tau$ ($y_i \in \mathbb{R}^p$). With hidden state h passed recurrently into the model at each time step, output predictions $o_i \in \mathbb{R}^p$ of the RNN are computed as follows [65]:

$$\begin{aligned} h_i &= \sigma(Ux_i + Wh_{i-1} + b), \\ o_i &= Vh_i + c, \end{aligned} \quad (44)$$

where $U \in \mathbb{R}^{m \times n}$ is the input weight matrix, $W \in \mathbb{R}^{m \times m}$ is the recurrent weight matrix, $h_{i-1} \in \mathbb{R}^m$ is the previous hidden state, $b \in \mathbb{R}^m$ is the input bias, $\sigma(\cdot)$ is a pointwise nonlinearity function, $h_i \in \mathbb{R}^m$ is the current hidden state, $V \in \mathbb{R}^{p \times m}$ is the output weight matrix, and $c \in \mathbb{R}^p$ is the output bias.

4.2.1 Orthogonal RNN (ORNN)

Denote \mathcal{L} as the objective function to be minimized, the gradient of the loss function for the hidden state is computed as:

$$\frac{\partial \mathcal{L}}{\partial h_i} = \frac{\partial \mathcal{L}}{\partial h_\tau} \cdot \frac{\partial h_\tau}{\partial h_i} = \frac{\partial \mathcal{L}}{\partial h_\tau} \cdot \prod_{j=i}^{\tau-1} \frac{\partial h_{j+1}}{\partial h_j} = \frac{\partial \mathcal{L}}{\partial h_\tau} \left(\prod_{j=i}^{\tau-1} D_{j+1} W^T \right), \quad (45)$$

where $D_{j+1} \in \mathbb{R}^{m \times m}$ is a diagonal matrix, whose entries consist of the derivate of the activation function. The pointwise non-linearity function $\sigma(\cdot)$ in Equation (44) is

suggested to be a rectified linear unit (ReLU) function [66, 67], whose output has a minimum value of 0. The input D_{j+1} has at least one non-zero entry of the derivative value for all j . Taking the Euclidean l_2 - norm to both sides of Equation (45), we have:

$$\left\| \frac{\partial \mathcal{L}}{\partial h_i} \right\|_2 \leq \left(\prod_{j=i}^{\tau-1} \|D_{j+1} W^T\|_2 \right) \left\| \frac{\partial \mathcal{L}}{\partial h_\tau} \right\|_2 = \left(\prod_{j=i}^{\tau-1} \|W\|_2 \right) \left\| \frac{\partial \mathcal{L}}{\partial h_\tau} \right\|_2 \quad (46)$$

If $\|W\|_2$ is greater than one, $\left\| \frac{\partial \mathcal{L}}{\partial h_i} \right\|_2$ grows exponentially as the increase of τ . As a result, the norm of the gradient in Equation (46) discloses the well-known gradient exploding problem that hinders the RNN from training [68]. If $\|W\|_2$ is smaller than one, $\left\| \frac{\partial \mathcal{L}}{\partial h_i} \right\|_2$ declines exponentially as the increase of τ , which leads to gradient vanishing problems [68].

A recent line of ORNNs imposes the orthogonal constraint on the hidden-to-hidden transformation of RNN. The recurrent weight transformation matrix W is restricted to be on the orthogonal manifold. Let A be an orthogonal matrix, for each vector X , its norm after orthogonal transformation is:

$$(AX)^T(AX) = X^T A^T A X = X^T X, \quad (47)$$

which means that orthogonal transformations do not change the norm of the original vector. As a result, $\left\| \frac{\partial \mathcal{L}}{\partial h_i} \right\|_2$ can remain invariant in ORNN when the transformation matrix W in Equation (46) is orthogonal. Therefore, the exploding and vanishing gradient problem of RNN can be alleviated. Moreover, orthogonal constraints can be generalized to unitary constraints in the complex domain.

4.2.2 Recent Advances of ORNN

uRNN [14] constructs a large unitary matrix by simple parametric unitary matrices, i.e., the unitary hidden-to-hidden matrix W is composed as follows,

$$W = D_3 R_2 F^{-1} D_2 \Pi R_1 F D_1, \quad (48)$$

where D is a diagonal matrix whose diagonal element $D_{j,j} = e^{i w_j}$ is defined by the imaginary unit i and parameters $w_j \in \mathbb{R}$, $R = I - 2 \frac{v v^*}{\|v\|^2}$ is a reflection matrix with the complex vector $v \in \mathbb{C}^n$, Π is a fixed random index permutation matrix, and F and F^{-1} are the Fourier and inverse Fourier transforms. In the matrix construction strategy like Equation (48), the number of parameters, memory, and computational overhead increase slowly at approximately linear speeds. Therefore, the training cost of large hidden layers can be reduced. In uRNN, a variation of the nonlinear activation ReLU named modReLU has been proposed to maintain the phase of complex-valued hidden states:

$$\sigma_{\text{modReLU}}(z) = \begin{cases} (|z| + b) \frac{z}{|z|}, & \text{if } |z| + b \geq 0 \\ 0, & \text{if } |z| + b \leq 0 \end{cases} \quad (49)$$

where $b \in \mathbb{R}$ is a bias parameter. uRNN defines a matrix U to map complex-valued hidden state h_t to real-valued output for prediction. The corresponding loss function is calculated as follows

$$o_t = U \begin{pmatrix} \text{Re}(h_t) \\ \text{Im}(h_t) \end{pmatrix} + b_o, \quad (50)$$

where b_o is the output bias, $\text{Re}(h_t)$ and $\text{Im}(h_t)$ represent the real and imaginary part of h_t respectively.

However, Wisdom et al. [69] noticed that the unitary parameter construction of Equation (48) cannot cover all $N \times N$ unitary matrices for $N > 7$, i.e., at least one $N \times N$ unitary matrix cannot be represented in the form of Equation (48). To address this problem, [69] designs a method to measure the representation capacity of the structured $N \times N$ unitary matrix. [69] comes up with a perspective that the unitary matrices parameterized by P real-valued parameters for $P \geq N^2$ is full-capacity, which means that it can cover all $N \times N$ unitary matrices.

Unlike generating compound orthogonal matrices with simple ones, the Lie exponential map can achieve orthogonal constraint on the hidden-to-hidden transformation [13]. The connected subjective exponential mapping $\exp : \mathfrak{g} \rightarrow G$ on the special orthogonal group is defined as

$$\exp(A) := I + A + \frac{1}{2}A^2 + \dots \quad (51)$$

Since it is a subjection, for each hidden-to-hidden transformation matrix W belonging to the special orthogonal group or unitary group, there must exist a skew-symmetric (or skew-Hermitian matrix) A that satisfies $\exp(A) = W$. Therefore, the hidden-to-hidden transformation $h_{t+1} = \sigma(W h_t + T x_{t+1})$ is equivalent to $h_{t+1} = \sigma(\exp(A) h_t + T x_{t+1})$. That is, the optimization on the orthogonal or unitary manifold can be transformed to the optimization in Euclidean space. Consequently, classic gradient descent optimizers such as Adam can be applied to minimize the loss function as well as satisfying orthogonal constraints. As a result, the Lie exponential map can achieve both cheap computation overhead and the mitigation of gradient exploding and vanishing problems.

Another method [70], which is based on the Lie group, defines a basis $\{T_j\}_{j=\{1, \dots, n^2\}}$ and coefficients $\{\lambda_j\}_{j=\{1, \dots, n^2\}}$ to construct the element $L \in \mathfrak{u}(n)$ as follows,

$$L = \sum_{j=1}^{n^2} \lambda_j T_j. \quad (52)$$

By using exponential mapping, the element U of corresponding unitary Lie group $U(n)$ can be represented as:

$$U = \exp(L) = \exp(\sum_{j=1}^{n^2} \lambda_j T_j). \quad (53)$$

Furthermore, Hyland et al. [70] offered an argument that the above parameterization helps generalize unitary RNN to arbitrary unitary matrices and figure out long-memory tasks.

Learning orthogonal filters in deep neural networks (DNN) can be formulated as an optimization problem over multiple dependent *Stiefel* manifolds (OMDSM) [71]. The

orthogonal linear module can substitute standard linear module in DNNs to stabilize the distributions of activation and regularize networks. Let W_k and b_k be learnable weight matrix and bias, parameter θ be $\{W_k, b_k | k = 1, 2, \dots, K\}$, the deep neural network can be represented as $f(x, \theta) : x \rightarrow \hat{y}$, where x is the input feature, and \hat{y} is the output prediction of DNN. The loss function is often designed as the discrepancy between label y and prediction values: $\mathcal{L}(y, f(x, \theta))$. Finally, the optimization problem is formulated as

$$\theta^* = \operatorname{argmin}_{\theta} \mathbb{E}_{(x,y) \in D} [\mathcal{L}(y, f(x, \theta))]. \quad (54)$$

OMDSM trains DNN with orthogonal weight matrix W_k in each layer. Thus, the optimization problem is reformulated as

$$\begin{aligned} \theta^* &= \operatorname{argmin}_{\theta} \mathbb{E}_{(x,y) \in D} [\mathcal{L}(y, f(x, \theta))] \\ \text{s.t. } W_k &\in \mathbb{O}_k^{n_k \times d_k}, k = 1, 2, \dots, K, \end{aligned} \quad (55)$$

where the matrix family $\mathbb{O}_k^{n_k \times d_k} = \{W_k \in \mathbb{R}^{n_k \times d_k} | W_k W_k^T = I\}$ is composed of multiple real *Stiefel* manifolds, which is an embedded sub-manifold of $\mathbb{R}^{n_k \times d_k}$. Each independent orthogonal filter $W \in \mathbb{R}^{n \times d}$ is given by the proxy parameter $V \in \mathbb{R}^{n \times d}$ as

$$W = PV, \quad (56)$$

where n is the number of output channels, d is the number of input channels, and $P \in \mathbb{R}^{n \times n}$ is the coefficient of the linear transformation. Firstly, V is centered by V_C :

$$V_C = V - c1_d^T, \quad (57)$$

where $c = \frac{1}{d}V1_d$ and 1_d is the d -dimension vector with all ones. Moreover, the eigenvalues Λ and eigenvectors D of the covariance matrix $V_C V_C^T$ are used to construct P :

$$P = D \Lambda^{-1/2} D^T. \quad (58)$$

Finally, W is formulated as

$$W = D \Lambda^{-1/2} D^T V_C. \quad (59)$$

Research has been conducted on exploring the influence of soft orthogonal constraints [72]. By allowing the diagonal elements of S to float around 1, the orthogonal transformation matrix W is relaxed as

$$W = USV^T, \quad (60)$$

where U and V are strict orthogonal matrices.

The above methods are mainly subject to $O(n^3)$ time complexity or dependent on complex matrices [73]. It is discovered that orthogonal matrices $W \subseteq O(2n)$ with doubled hidden size, can substitute complex or unitary matrices in $\mathbb{C}^{n \times n}$. Inspired by the above discovery, [73] proposed to utilize Householder matrices to achieve parametrization of orthogonal transition matrices. As a result, complex matrices are unneeded and time complexity is reduced, while the effect is similar to the unitary constraint.

The norm-keeping property of orthogonal matrices may make ORNN have difficulty paying little attention to extraneous information [74]. To relieve this problem, Jing et al. [74] put forward the gated orthogonal recurrent unit (GORU) to be unconcerned with irrelevant or noise information while learning long-term dependencies. By adding the gating mechanism, experiment results demonstrate that GORU outperforms the unitary RNN on natural language processing tasks such as question answering tasks, together with long-term dependency tasks such as denoising and copying tasks.

In summary, uRNN [14] parameterizes the unitary hidden-to-hidden matrix by composing simple unitary matrices. However, the above parameterization cannot cover all $N \times N$ unitary matrices. To make up for that, full-capacity uRNN [69] is put forward. Unlike uRNN, expRNN [13] exploits the exponential map to achieve orthogonal constraints more easily. Furthermore, OMDSM innovatively uses re-parameterization to optimize DNN over multiple dependent *Stiefel* manifolds instead of one manifold [71]. Moreover, research has explored whether and how the hard orthogonal constraints on RNN can be relaxed [72]. By creatively introducing the householder matrix, the considerable time complexity of parameterizing unitary matrices can be mitigated [73]. Last but not least, GORU [74] designs a forget gate, so that ORNN can pay little attention to extraneous information.

4.3 Geometric GNN

GNN can be used to construct a learning network based on irregular graphs. Each graph is represented by vertexes and edges, which describes the relationship between vertexes. GNN encodes vertexes as feature vectors and models edges as a relationship matrix between vertexes. In GNN, graph convolution is performed between the relationship matrix and the feature matrix. Therefore, GNN can take advantage of the graph structure and update the feature information of each vertex iteratively. Endowing Euclidean GNN with hyperbolic geometry can make it superior in capturing graph structure [52]. Recently, plenty of geometric GNN research has investigated how to incorporate GNN with hyperbolic manifold to benefit from a neighborhood with a highly organized structure.

To make full use of the rich geometric information in the graph, geometry interaction learning (GIL) [53] incorporates Euclidean space with hyperbolic geometry by exponential and logarithmic transformations. Moreover, learnable message passing parameters are optimized on the *Möbius* manifold. To allow each node to determinate the importance of each geometry space freely, the GIL framework employs a flexible dual-space to model both low-dimensional regular data and complex hierarchical structures. A broad spectrum of experiments show that the GIL method is adaptative to node classification and link prediction tasks.

Observing that GCN cannot cope with changes in static structure information, Liu et al. [75] put forward a manifold regularized dynamic graph convolutional network (MRDGCN), which integrated manifold regularization into GCN to model dynamic structure information. MRDGCN automatically updates the structure information before convergence, which makes up for GCN’s inability to remain optimal in pace with the learning process. Considerable comparative experiments on human activity datasets

and citation network datasets evaluate that MRDGCN outperforms GCN and other semi-supervised learning methods.

4.4 Geometric Optimization for Other Deep Learning Methods

Robust Time Series Prediction. Considering that noises and outliers are inevitable and important for system modeling, Feng et al. [76] put forward a robust manifold broad learning system (RM-BLS) for time series prediction with large-scale noisy disturbances. RM-BLS applies low-rank constraint so that features spoiled by perturbations can be abandoned by feature selection. Furthermore, RM-BLS can also abandon features that are not satisfied to low-dimensional manifold embedding. In addition to the low-rank manifold, [76] also considers Stiefel manifold optimization and satisfies orthogonal constraints by Cayley transformation and curvilinear search algorithm.

Medical Reconstruction. Geometric optimization have played an essential role in the medical field, such as magnetic resonance imaging (MRI) for cardiac diagnosis. Dynamic MR can be optimized on a low-rank tensor manifold [77] to seize the powerful temporal connection between dynamic signals. Moreover, the iterative reconstruction process is flattened to a neural network for acceleration, called dubbed Manifold-Net. To recover free breathing and ungated cardiac MRI data, Biswas et al. [78] creatively combined CNN with smoothness regularization on manifolds (SToRM) prior. The Laplacian matrix L in SToRM $tr(X^T L X)$ is defined on the manifold to model similarities between data beyond the ambient space. To utilize the manifold structure and patient-specific information, data denoising based on CNN and SToRM together with conjugate gradients (CG) step take place alternatively. Experiments confirm that combining CNN with SToRM leads to a fast and high quality reconstruction of MRI data even when the down sampling frequency is less than 8.2s of acquisition time per slice.

Transfer Learning. To maximize the utilization of finite computing resources, transfer learning aims to reuse the neural network, which is trained for task A , to address a similar task B . Knowledge distillation (KD) is intended to transfer model knowledge from a well-trained model (teacher) to a compact model (student) with soft labels. Zhang et al. [79] devised an end-to-end deep manifold-to-manifold transforming network (DMT-Net) for discriminative feature learning. However, reconstructing a more discriminative SPD manifold from the original one is challenging. DMT-Net designs a local SPD convolutional layer and the non-linear SPD activation layer to deal with it. Huang et al. [80] designed a manifold-to-manifold transformation matrix W and constrained the optimization to reside on the SPD manifold. Moreover, the intra-class and inter-class dissimilarity graphs are built under W . Hence, they can represent local geometry structures and learn the discriminative feature of SPD data.

Optimal Transport. Optimal transport aims to measure the distance between two probability distributions by using transport plan Γ and cost matrix C , i.e.,

$$\min_{\Gamma \in \Pi(\mu_1, \mu_2)} \text{trace}(\Gamma^T C), \quad (61)$$

where $\Pi(\mu_1, \mu_2)$ consists of joint distributions with marginals μ_1 and μ_2 . Supposing μ_1 has m points and μ_2 has n points, the size of both Γ and C is $m \times n$. There are

works that have explored the application of geometric optimization in optimal transport problems [81]. By using the Riemannian gradient descent (RGD) algorithm, [82] explored how to convert optimal transport problems with different regularizations to the optimization problem on the coupling matrix manifold (CMM). To clarify the geometry optimization process, [82] took classic optimal transport problems (e.g., the entropy-regularized [83] and power-regularized optimal transport problems [84]) as an example. Observing that the constrained set $\Pi(\mu_1, \mu_2)$ has a differentiable manifold structure, [85] and [86] solved the optimal transport problem on a generalized doubly stochastic manifold, broadening the application of manifold geometry in non-linear optimal transport problems. In addition to general problems, [86] discusses how to adapt the above geometric optimization framework to particular ones, such as problems with sparse optimal transport map and problems of how to learn multiple transport plans simultaneously.

Robots. Bayesian optimization is an important technology for robots since it is effective in solving optimization problems such as controller tuning, policy adaptation, and robot design. Bayesian optimization is based on the Gaussian Process that relies on domain knowledge exploration. Therefore, geometry-aware Bayesian optimization emerges as a promising paradigm that can incorporate domain geometry into the optimization algorithm. There are many commonly used kernels in Gaussian Process, among which Matérn kernel is used to study geometry-aware Gaussian process and Bayesian optimization. Euclidean Matérn kernel is defined as follows,

$$K(x, x') = \exp\left(-\frac{\|x - x'\|^2}{2\sigma^2}\right), \quad (62)$$

where σ is a free parameter. Matérn kernel is a commonly used kernel function when constructing stationary Gaussian process. Borovitskiy et al. [87] pointed out that generalizing the Matérn kernel to the Riemannian manifold merely by replacing Euclidean norms $\|x - x'\|^2$ with geodesic distances $d_g(x - x')$ could not produce a well-defined kernel function. To construct the Riemannian Matérn kernel defined by stochastic partial differential equations, Borovitskiy et al. proposed to obtain Laplace–Beltrami eigenpairs for the specific manifold and approximate the infinite sum, which forms the basis for geometry-aware Bayesian optimization on robotics. However, the above method suffers from two problems [88], i.e., i) the amount of computation increases exponentially with the manifold dimension; and ii) such method is inapplicable to non-compact manifolds. To address these problems, Jaquier et al. [88] observed a general expression of Matérn kernels, which is helpful to generalize them to the torus and sphere manifold. More importantly, Matérn kernels can be generalized to non-compact manifolds (e.g., SPD matrix manifold and the Hyperbolic space) by using the general expression.

Continual learning. Continual learning aims to remember and use the experience of previous tasks to learn new tasks, which raises requirements for the memory ability of neural networks. Chaudhry et al. [89] proposed to achieve the purpose of continual learning on the low-rank orthogonal manifold. The core idea of this method is to project the gradient into disjoint low-rank orthogonal subspace by introducing task-specific projection matrix in the last second layer, which can make the gradient between different tasks orthogonal and alleviate catastrophic forgetting. The concept

of gradient orthogonality was first proposed in [90]. The essential reason for catastrophic forgetting is that learning new tasks will affect the parameters learned on the old tasks. Updating parameters in the direction orthogonal to the gradient of the old tasks can not only learn new tasks but also keep the loss of the old tasks, which alleviates catastrophic forgetting. In the deep neural network, the chain derivation process can be approximately regarded as the linear transformation of the gradient, which will destroy the orthogonality of the gradient of the earlier layers and lead to catastrophic forgetting. To ensure the orthogonality of the gradient between different tasks, [89] constrains parameters on the *Stiefel* manifold, making this linear transformation an orthogonal transformation.

5 Toolbox

The success of the Tensorflow platform and PyTorch framework in deep learning shows that toolboxes can conveniently help build neural networks. There are valuable toolboxes designed for quickly setting up manifolds optimization. Manopt [91], Pymanopt [92], McTorch [93], and Geomstats [94] are classic toolboxes that implement manifold geometries and optimization algorithms. Moreover, they are user-friendly and time-saving. Table 2 compares these toolboxes from the aspect of applicable manifolds and geometry operations.

Manopt, which is built on Matlab, is a helpful tool to handle a variety of geometry constraints (e.g., different manifold structures introduced in 2.3). A Riemannian optimization in Manopt [91] is designed as a problem including manifold structures that the search space is confined to. The cost function, or optimization object, is included in the above optimization problem as well. If needed, a problem structure can also cover derivatives of the objective function. In Manopt, solvers are functions that give a general implementation to Riemannian optimization algorithms, including steepest-descent, conjugate-gradient, and Riemannian trust-regions algorithms. Since solvers in Manopt is designed to minimize the cost function, the cost function should be multiplied by a negative one if it is a maximization problem.

Pymanopt [92] extends Manopt to python. Similar to the usage of Manopt in Matlab, a Riemannian optimization in Pymanopt should be initialized with a predefined manifold and cost function. Equipped with different solvers, the optimization process and result can be diverse. Pymanopt covers all sorts of smooth manifolds such as the oblique manifold, sphere manifold, and *Graßmann* manifold. Numerable optimization algorithms are included as solvers, for instance, trust-regions, conjugate-gradient, and steepest-descent algorithms are contained by Pymanopt.

Manopt and Pymanopt are limited to shallow learning optimizations and are not applicable to deep learning optimizations. To fill the deficiency of Manopt and Pymanopt, McTorch has been implemented by extending Pytorch [93], a handy framework for deep learning. As a result, it implements a general solution for deep learning optimizations on the manifold. Unlike Manopt and Pymanopt, Riemannian optimization in McTorch does not need to define problems, manifolds, and solvers. Similar to Pytorch, Riemannian optimization in McTorch only needs to define modules and optimizers such as Adam. Network modules inherited from *torch.nn.module* initialize

layers with manifolds and forward functions.

Geopt [95], which is implemented on top of Pytorch, has a cheaper infrastructure cost than McTorch. Extended from `torch.nn.Module.parameters`, Geopt supports tensors and parameters on the manifold. Moreover, Geopt provides Riemannian optimizers, for instance, `RiemannianSGD` and `RiemannianAdam` are available and inherited from `torch.optim.SGD` and `torch.optim.Adam`, respectively [95].

Another toolbox, Geomstats, is composed of two core modules, i.e., geometry and learning [94]. The former implements Riemannian metrics, including geodesic distance. The latter implements statistics and learning algorithms inherited from Scikit-Learn classes such as *K-Means* and PCA. Compared with Geomstats, other toolboxes mentioned are less modular and lack statistical learning algorithms. Taking clustering, one of the classic statistical learning problems, as an example, Geomstats encapsulates the class *Online K-Means* with the parameter *metric*. To perform clustering operation, users only need to initialize the Riemannian metric and call *fit* function of class *Online K-Means* as they do in Scikit-Learn, which is easy and convenient.

TheanoGeometry [96] uses Theano, a python-based and research-oriented framework, to implement differential geometry and non-linear statistics problems. TheanoGeometry outperforms other manifold toolboxes since it can handle symbolic calculations. Thus, Theano code can be generated from symbolic expression directly, where non-linear symbolic statistics can be optimized with a trivial amount of code. TheanoGeometry goes further beyond efficient symbolic computation. It implements Riemannian geometry such as geodesic equations, parallel transport, and curvature with automatic differentiation features [97].

6 Performance Evaluation

Table 4, 5, 6, 7, 8 compare the performance of aforementioned geometric optimization methods on various visual tasks (e.g., character recognition, emotion recognition, act recognition, and scene recognition tasks). Each image dataset used in different visual tasks is summarized in Table 3.

Table 4 shows that GORU [74] outperforms other ORNNs on the MNIST dataset. GORU adds a forget gate, which enables ORNN to filter out irrelevant information. Taking advantage of the surjective exponential map, `expRNN` [13] realizes orthogonal parameterization with a more straightforward way. Unlike `expRNN`, `uRNN` [14] uses simple unitary matrices to construct the unitary hidden-to-hidden matrix. However, such matrix construction method fails to represent all $N \times N$ unitary matrices. Therefore, Scott Wisdom et al. [69] proposed full-capacity `uRNN` to overcome that bottleneck of `uRNN`. Using regularization terms to realize orthogonal parameterization, `soRNN` [72] explores the effect of soft orthogonal constraints on RNN. `ORNN` [73] exploits the householder matrix to enforce an orthogonal constraint on RNN, which mitigates the considerable time complexity of unitary matrices. Table 4 shows that combining the forget gate, or noise filter, with ORNN improves the performance of ORNN.

Table 5 shows that SPDNet [50] and GrNet [51] can achieve better classification results than state-of-the-art methods on AFEW dataset [99]. The following methods for

comparison are shallow learning methods applying manifold structure: Expression-lets on Spatio-Temporal Manifold (STM-ExpLet) [107], Riemannian Sparse Representation combining with Manifold Learning on the manifold of SPD matrices (RSR-SPDML) [32], Discriminative Canonical Correlations (DCC) [109], *Graßmann* Discriminant Analysis (GDA) [56], Grassmannian Graph-Embedding Discriminant Analysis (GGDA) [118], and Projection Metric Learning (PML) [110]. Deep Second-order Pooling (DeepO2P) [108] is a traditional CNN model using the standard optimization method. SPDNet exploits the *Stiefel* manifold parameterization by BiMap layers and introduces non-linearity into the network by ReEig layers. Experiments prove that using the manifold geometry in deep learning optimization can improve network performance. The LogEig layer is crucial to Riemannian computing and contributes to the emotion classification success of SPDNet. The success of GrNet shows that optimizing on the *Graßmann* manifold and building a geometry-aware deep learning network is significant for learning representative features and classifying emotions with a relatively high level of accuracy.

Table 5 presents that the manifold-based classification method proposed by Hariri et al. [59] achieves the highest precision on BU-3DFE and Bosphorus datasets. Hariri et al. used a Graph-Matching kernel and classified facial expression data with SPD covariance descriptors. It outperforms Tree-PNN [111] and XP Huynh [113] on the BU-3DFE dataset by a narrow margin, and the latter two methods use traditional CNN. The manifold-based method proposed by Hariri et al. greatly exceeds the methods proposed by Stefano Berretti [112] and Amal Azazi [114] by approximately 15% and 8% on BU-3DFE dataset. In particular, the latter two methods apply SIFT and Speed Up Robust Features descriptors. On the Bosphorus dataset, the classification accuracy of Hariri et al.’s method [59] is almost far higher than all state-of-the-art methods. For example, it is even 30% better than the ZernikeMoments [117]. The low-accuracy methods use local features rather than SPD covariance matrices. Overall, these results indicate that using geometry constraints is vital for feature representation and emotion recognition.

Table 6 shows that SPDNet achieves the highest accuracy on the action recognition task, followed by GrNet. As Table 7 shows, SPDNet and GrNet outperform state-of-the-art methods on the face recognition task. The eigenvalue decomposition in SPDNet introduces non-linearity and the QR decomposition in GrNet performs orthonormalization, both of which contribute to the classification accuracy. Therefore, using matrix decomposition is vital for exploring manifold constrained parameters. The success of the deep manifold network on the action recognition and face recognition task shows that optimizing deep learning on the manifold helps learn favorable features and classify human actions better.

As shown in Table 8, Scene Recognition by Manifold Regularized Deep Learning Architecture (SRMR) [60] outperforms state-of-the-art non-manifold methods on all three scene recognition datasets. Lazebnik et al. [120] partitioned images into fine subregions for image matching. Dixit et al. [121] formulated Bayesian adaptation for scene image classification. Kwitt et al. [122] recognized scene images on the statistical (semantic) manifold. From the perspective of information geometry, they can consider the parameter vectors as Riemannian manifolds. Goh et al. [123] used SIFT descriptors and represented vectorially for image recognition. Li et al. [104]

interpreted the semantic components of images. Wu and Rehg [124] used the Histogram Intersection Kernel (HIK) for sports game classification. Donahue et al. [124] used extracted features for novel generic tasks. SRMR’s incredible success on scene recognition tasks shows that manifold regularizations are significant for improving the classification accuracy of deep learning. Experimental results vary with different network architecture settings for the same manifold constrained method. For example, SPDNet [50] has four different architecture configurations: i) SPDNet-0BiRe without using blocks of BiMap/ReEig, ii) SPDNet-1BiRe using 1 block of BiMap/ReEig, iii) SPDNet-2BiRe using 2 blocks of BiMap/ReEig, and iv) SPDNet-3BiRe using 3 blocks of BiMap/ReEig. GrNet [51] has three different configurations: i) GrNet-0Block without using blocks of Projection-Pooling, ii) GrNet-1Block using 1 block of Projection-Pooling, and iii) GrNet-2Block using 2 blocks of Projection-Pooling. These methods studied how different architecture settings affected classification accuracy. Note that our article follows the raw settings reported from corresponding articles. On that account, this article did not present classification accuracy under different architecture configurations.

7 Conclusions and Future Work

In this article, a survey on recent advances in applying geometric optimization to deep learning is presented. This article reviewed progress of optimizing deep learning networks on manifolds according to the classification of deep learning backbones (e.g., CNN, RNN, and GNN). In particular, this article discussed the theory and toolboxes for geometric optimization. Although geometric optimization brings various advantages to deep learning methods, it still suffers from the following challenges.

- **Dataset-Oriented Geometric Optimization.** Various methods (e.g., uRNN [14] and Cheap Orthogonal Constraints in Neural Networks [13]) utilize small image datasets such as MNIST handwritten digits to validate the effectiveness of geometric optimization. Whether geometric optimization can achieve good performance on enormous and complicated datasets such as Penn Tree Bank (PTB) needs further research. This prompts researchers to use more challenging datasets to verify the performance of deep learning techniques after applying geometric optimization.
- **Model-Oriented Geometric Optimization.** Although optimizing deep learning networks such as CNN and RNN on the Riemannian manifold has been proven successful, geometric optimization has not been applied to all deep learning methods. For example, there is a lack of research in optimizing reinforcement learning and federated learning on manifolds, which is crucial in automatic control and privacy protection. This forces researchers to further explore the potential and benefit of optimizing more deep learning networks from a geometric perspective.
- **Manifold-Oriented Geometric Optimization.** Manifold geometry plays an important role in geometric optimization and different manifolds have different applications. For instance, the orthogonal manifold can be used to alleviate feature redundancy and oblique manifold can be utilized for optimizing dictionary learning.

However, applications of certain manifolds such as centered matrix manifold remain blank in the literature. This motivates researchers to exploit and use manifold structures for geometric optimization applications as much as possible.

This article demonstrated that geometric optimization can grasp advantage of the geometry information of search space, speed up the optimization process, and mitigate gradient explosion and vanishing problems. However, considering unexplored deep learning methods such as reinforcement learning, together with unused manifold structures such as centered matrix manifold, it is still a huge challenge to push the boundaries of geometric optimization in deep learning.

References

- [1] Ian Goodfellow, Yoshua Bengio, Aaron Courville, and Yoshua Bengio. *Deep learning*. 2016.
- [2] Raphael JL Townshend, Stephan Eismann, Andrew M Watkins, Ramya Rangan, Maria Karelina, Rhiju Das, and Ron O Dror. Geometric deep learning of mra structure. *Science*, 373(6558):1047–1051, 2021.
- [3] Mingxing Tan and Quoc Le. Efficientnet: Rethinking model scaling for convolutional neural networks. In *International Conference on Machine Learning (ICML)*, pages 6105–6114, 2019.
- [4] Zhen He, Shaobing Gao, Liang Xiao, Daxue Liu, Hangen He, and David Barber. Wider and deeper, cheaper and faster: Tensorized lstms for sequence learning. In *Advances in Neural Information Processing Systems*, pages 1–11, 2017.
- [5] David Rolnick and Max Tegmark. The power of deeper networks for expressing natural functions. In *International Conference on Learning Representations (ICLR)*, 2018.
- [6] Jiayun Wang, Yubei Chen, Rudrasis Chakraborty, and Stella X Yu. Orthogonal convolutional neural networks. In *Proceedings of the IEEE Conference on Computer Vision and Pattern Recognition (CVPR)*, pages 11505–11515, 2020.
- [7] M. Storath and A. Weinmann. Variational regularization of inverse problems for manifold-valued data. *Information and Inference: A Journal of the IMA*, 10(1):195–230, 2021.
- [8] P-A Absil, Robert Mahony, and Rodolphe Sepulchre. *Optimization algorithms on matrix manifolds*. 2008.
- [9] Nicolas Boumal. An introduction to optimization on smooth manifolds. Available online, Aug 2020.
- [10] Jiang Hu, Xin Liu, Zai-Wen Wen, and Ya-Xiang Yuan. A brief introduction to manifold optimization. *Journal of the Operations Research Society of China*, 8(2):199–248, 2020.

- [11] Xian Wei. *Learning Image and Video Representations Based on Sparsity Priors*. 2017.
- [12] Nitin Bansal, Xiaohan Chen, and Zhangyang Wang. Can we gain more from orthogonality regularizations in training deep cnns. In *Proceedings of the International Conference on Neural Information Processing Systems*, pages 4266–4276, 2018.
- [13] Mario Lezcano-Casado and David Martinez-Rubio. Cheap orthogonal constraints in neural networks: A simple parametrization of the orthogonal and unitary group. In *International Conference on Machine Learning (ICML)*, pages 3794–3803, 2019.
- [14] Martin Arjovsky, Amar Shah, and Yoshua Bengio. Unitary evolution recurrent neural networks. In *International Conference on Machine Learning (ICML)*, pages 1120–1128, 2016.
- [15] Yanhong Fei, Yingjie Liu, Xian Wei, and Mingsong Chen. O-vit: Orthogonal vision transformer. *arXiv preprint arXiv:2201.12133*, 2022.
- [16] J. Zhou, M. N. Do, and J Kovačević. Ieee transactions on image processing 1 special paraunitary matrices, cayley transform, and multidimensional orthogonal filter banks. *IEEE Transactions on Image Processing*, 14(6):760, 2008.
- [17] P Rodríguez, J González, G. Cucurull, J. M. Gonfaus, and X. Roca. Regularizing cnns with locally constrained decorrelations. 2017.
- [18] Jorge Nocedal and Stephen Wright. *Numerical optimization*. 2006.
- [19] David G Luenberger, Yinyu Ye, et al. *Linear and nonlinear programming*, volume 2. 1984.
- [20] Daniel Gabay. Minimizing a differentiable function over a differential manifold. *Journal of Optimization Theory and Applications*, 37(2):177–219, 1982.
- [21] Roger W Brockett. Differential geometry and the design of gradient algorithms. In *Proc. Symp. Pure Math., AMS*, pages 69–92, 1993.
- [22] Alan Edelman, Tomás A Arias, and Steven T Smith. The geometry of algorithms with orthogonality constraints. *SIAM journal on Matrix Analysis and Applications*, 20(2):303–353, 1998.
- [23] Simon Hawe, Matthias Seibert, and Martin Kleinsteuber. Separable dictionary learning. In *Proceedings of the IEEE Conference on Computer Vision and Pattern Recognition (CVPR)*, pages 438–445, June 2013.
- [24] Xian Wei, Hao Shen, and Martin Kleinsteuber. Trace quotient meets sparsity: A method for learning low dimensional image representations. In *Proceedings of the IEEE Conference on Computer Vision and Pattern Recognition (CVPR)*, pages 5268–5277, 2016.

- [25] P-A Absil, Christopher G Baker, and Kyle A Gallivan. Trust-region methods on riemannian manifolds. *Foundations of Computational Mathematics*, 7(3):303–330, 2007.
- [26] Jean-Pierre Dedieu, Pierre Priouret, and Gregorio Malajovich. Newton’s method on riemannian manifolds: covariant alpha theory. *IMA Journal of Numerical Analysis*, 23(3):395–419, 2003.
- [27] Xian Wei, Yuanxiang Li, Hao Shen, Fang Chen, Martin Kleinsteuber, and Zhongfeng Wang. Dynamical textures modeling via joint video dictionary learning. *IEEE Transactions on Image Processing*, 26(6):2929–2943, 2017.
- [28] Simon Alois Hawe. *Learning sparse data models via geometric optimization with applications to image processing*. PhD thesis, Technische Universität München, 2013.
- [29] S. Kumar, Z. Mhammedi, and M. Harandi. Geometry aware constrained optimization techniques for deep learning. In *Proceedings of the IEEE Conference on Computer Vision and Pattern Recognition (CVPR)*, pages 4460–4469, 2018.
- [30] John M Lee. Smooth manifolds. In *Introduction to Smooth Manifolds*, pages 1–31. Springer, 2013.
- [31] Diego Tosato, Michela Farenzena, Mauro Spera, Vittorio Murino, and Marco Cristani. Multi-class classification on riemannian manifolds for video surveillance. In *ECCV*, pages 378–391, 2010.
- [32] Mehrtash T Harandi, Mathieu Salzmann, and Richard Hartley. From manifold to manifold: Geometry-aware dimensionality reduction for spd matrices. In *European Conference on Computer Vision (ECCV)*, pages 17–32, 2014.
- [33] Zhiwu Huang, Ruiping Wang, Shiguang Shan, Xianqiu Li, and Xilin Chen. Log-euclidean metric learning on symmetric positive definite manifold with application to image set classification. In *Proceedings of International Conference on Machine Learning (ICML)*, volume 37, pages 720–729, 2015.
- [34] Jieping Ye and Qi Li. Lda/qr: an efficient and effective dimension reduction algorithm and its theoretical foundation. *Pattern Recognition*, 37(4):851–854, 2004.
- [35] John NR Jeffers. Two case studies in the application of principal component analysis. *Journal of the Royal Statistical Society: Series C (Applied Statistics)*, 16(3):225–236, 1967.
- [36] Svante Wold, Kim Esbensen, and Paul Geladi. Principal component analysis. *Chemometrics and Intelligent Laboratory Systems*, 2(1-3):37–52, 1987.
- [37] Hui Zou and Lingzhou Xue. A selective overview of sparse principal component analysis. *Proceedings of the IEEE*, 106(8):1311–1320, 2018.

- [38] Frank Rehm, Frank Klawonn, and Rudolf Kruse. Mds polar: A new approach for dimension reduction to visualize high dimensional data. In *International Symposium on Intelligent Data Analysis*, pages 316–327, 2005.
- [39] Andreas Buja, Deborah F Swayne, Michael L Littman, Nathaniel Dean, Heike Hofmann, and Lisha Chen. Data visualization with multidimensional scaling. *Journal of Computational and Graphical Statistics*, 17(2):444–472, 2008.
- [40] Mingyu Fan, Hong Qiao, Bo Zhang, and Xiaoqin Zhang. Isometric multi-manifold learning for feature extraction. In *International Conference on Data Mining*, pages 241–250. IEEE, 2012.
- [41] Yepeng Ni, Jianping Chai, Yan Wang, and Weidong Fang. A fast radio map construction method merging self-adaptive local linear embedding (lle) and graph-based label propagation in wlan fingerprint localization systems. *Sensors*, 20(3):767, 2020.
- [42] Bo Li, Yan-Rui Li, and Xiao-Long Zhang. A survey on laplacian eigenmaps based manifold learning methods. *Neurocomputing*, 335:336–351, 2019.
- [43] Rong Wang, Feiping Nie, Richang Hong, Xiaojun Chang, Xiaojun Yang, and Weizhong Yu. Fast and orthogonal locality preserving projections for dimensionality reduction. *IEEE Transactions on Image Processing*, 26(10):5019–5030, 2017.
- [44] Effrosini Kokiopoulou, Jie Chen, and Yousef Saad. Trace optimization and eigenproblems in dimension reduction methods. *Numerical Linear Algebra with Applications*, 18(3):565–602, 2011.
- [45] Albert Tarantola. *Inverse problem theory and methods for model parameter estimation*. 2005.
- [46] Simon Hawe, Martin Kleinsteuber, and Klaus Diepold. Analysis operator learning and its application to image reconstruction. *IEEE Transactions on Image Processing*, 22(6):2138–2150, 2013.
- [47] W. P. Krijnen. Positive loadings and factor correlations from positive covariance matrices. *Psychometrika*, 69(4):655–660, 2004.
- [48] Pavan Turaga and Rama Chellappa. Locally time-invariant models of human activities using trajectories on the grassmannian. In *Proceedings of the IEEE Conference on Computer Vision and Pattern Recognition (CVPR)*, pages 2435–2441, 2009.
- [49] M. Ozay and Takayuki Okatani. Optimization on submanifolds of convolution kernels in cnns. *ArXiv*, abs/1610.07008:arXiv-1610, 2016.
- [50] Z. Huang and L. Gool. A riemannian network for spd matrix learning. In *Proceedings of the 31st AAAI Conference on Artificial Intelligence (AAAI)*, pages 2036–2042, 2017.

- [51] Z. Huang, Jiqing Wu, and L. Gool. Building deep networks on grassmann manifolds. In *Proceedings of the AAAI Conference on Artificial Intelligence (AAAI)*, pages 3279–3286, 2018.
- [52] Qi Liu, Maximilian Nickel, and Douwe Kiela. Hyperbolic graph neural networks. *Advances in Neural Information Processing Systems*, 32:8230–8241, 2019.
- [53] Shichao Zhu, Shirui Pan, Chuan Zhou, Jia Wu, Yanan Cao, and Bin Wang. Graph geometry interaction learning. In *Advances in Neural Information Processing Systems*, volume 33, pages 7548–7558, 2020.
- [54] Rahul Chauhan, Kamal Kumar Ghanshala, and RC Joshi. Convolutional neural network (cnn) for image detection and recognition. In *International Conference on Secure Cyber Computing and Communication (ICSCCC)*, pages 278–282. IEEE, 2018.
- [55] Aliasghar Mortazi and Ulas Bagci. Automatically designing cnn architectures for medical image segmentation. In *International Workshop on Machine Learning in Medical Imaging*, pages 98–106, 2018.
- [56] Jihun Hamm and Daniel D Lee. Grassmann discriminant analysis: a unifying view on subspace-based learning. In *Proceedings of the 25th International Conference on Machine Learning (ICML)*, pages 376–383, 2008.
- [57] Lei Zhang, Xiantong Zhen, Ling Shao, and Jingkuan Song. Learning match kernels on grassmann manifolds for action recognition. *IEEE Transactions on Image Processing*, 28(1):205–215, 2019.
- [58] Mengyi Liu, Ruiping Wang, Shaoxin Li, Shiguang Shan, Zhiwu Huang, and Xilin Chen. Combining multiple kernel methods on riemannian manifold for emotion recognition in the wild. In *Proceedings of International Conference on multimodal interaction*, pages 494–501, 2014.
- [59] Walid Hariri and Nadir Farah. Efficient graph-based kernel using covariance descriptors for 3d facial expression classification. In *Proceedings of International Conference on Intelligent Systems and Pattern Recognition*, pages 7–11, 2020.
- [60] Yuan Yuan, Lichao Mou, and Xiaoqiang Lu. Scene recognition by manifold regularized deep learning architecture. *IEEE Transactions on Neural Networks and Learning Systems*, 26(10):2222–2233, 2015.
- [61] Chaoqun Hong, Jun Yu, Jian Zhang, Xiongnan Jin, and Kyong-Ho Lee. Multi-modal face-pose estimation with multitask manifold deep learning. *IEEE Transactions on Industrial Informatics*, 15(7):3952–3961, 2018.
- [62] Jean-Michel Roufosse, Abhishek Sharma, and Maks Ovsjanikov. Unsupervised deep learning for structured shape matching. In *Proceedings of the IEEE/CVF International Conference on Computer Vision (ICCV)*, pages 1617–1627, 2019.

- [63] Zhiwu Huang, Chengde Wan, Thomas Probst, and Luc Van Gool. Deep learning on lie groups for skeleton-based action recognition. In *Proceedings of the IEEE Conference on Computer Vision and Pattern Recognition (CVPR)*, pages 6099–6108, 2017.
- [64] Xin Chen, Jian Weng, Wei Lu, Jiaming Xu, and Jiasi Weng. Deep manifold learning combined with convolutional neural networks for action recognition. *IEEE Transactions on Neural Networks and Learning Systems*, 29(9):3938–3952, 2017.
- [65] Razvan Pascanu, Çağlar Gülçehre, Kyunghyun Cho, and Yoshua Bengio. How to construct deep recurrent neural networks. *ArXiv*, abs/1312.6026:arXiv-1312, 2014.
- [66] Xavier Glorot, Antoine Bordes, and Yoshua Bengio. Deep sparse rectifier neural networks. In *Proceedings of International Conference on Artificial Intelligence and Statistics*, pages 315–323, 2011.
- [67] Vinod Nair and Geoffrey E. Hinton. Rectified linear units improve restricted boltzmann machines. In *Proceedings of the International Conference on International Conference on Machine Learning*, page 807–814, 2010.
- [68] Sekitoshi Kanai, Yasuhiro Fujiwara, and Sotetsu Iwamura. Preventing gradient explosions in gated recurrent units. In *Proceedings of the 31st International Conference on Neural Information Processing Systems*, pages 435–444, 2017.
- [69] Scott Wisdom, Thomas Powers, John Hershey, Jonathan Le Roux, and Les Atlas. Full-capacity unitary recurrent neural networks. 10 2016.
- [70] Stephanie L Hyland and Gunnar Rätsch. Learning unitary operators with help from $u(n)$. In *Proceedings of the Thirty-First AAAI Conference on Artificial Intelligence*, pages 2050–2058, 2017.
- [71] Lei Huang, Xianglong Liu, Bo Lang, Adams Wei Yu, Yongliang Wang, and Bo Li. Orthogonal weight normalization: Solution to optimization over multiple dependent stiefel manifolds in deep neural networks. In *Proceedings of the AAAI Conference on Artificial Intelligence (AAAI)*, pages 3271–3278, 2018.
- [72] Eugene Vorontsov, Chiheb Trabelsi, Samuel Kadoury, and Chris Pal. On orthogonality and learning recurrent networks with long term dependencies. In *International Conference on Machine Learning (ICML)*, pages 3570–3578, 2017.
- [73] Zakaria Mhammedi, Andrew Hellicar, Ashfaqur Rahman, and James Bailey. Efficient orthogonal parametrisation of recurrent neural networks using householder reflections. In *International Conference on Machine Learning (ICML)*, pages 2401–2409. PMLR, 2017.
- [74] Li Jing, Çağlar Gulcehre, John Peurifoy, Yichen Shen, Max Tegmark, Marin Soljatic, and Yoshua Bengio. Gated orthogonal recurrent units: On learning to forget. *Neural Computation*, 31(4):765–783, 2019.

- [75] Weifeng Liu, Sichao Fu, Yicong Zhou, Zheng-Jun Zha, and Liqiang Nie. Human activity recognition by manifold regularization based dynamic graph convolutional networks. *Neurocomputing*, 444:217–225, 2021.
- [76] Shoubo Feng, Weijie Ren, Min Han, and Yen Wei Chen. Robust manifold broad learning system for large-scale noisy chaotic time series prediction: A perturbation perspective. *Neural Networks*, 117:179–190, 2019.
- [77] Ziwen Ke, Zhuoxu Cui, Wenqi Huang, Jing Cheng, Seng Jia, Haifeng Wang, Xin Liu, Hairong Zheng, Leslie Ying, Yanjie Zhu, and Dong Liang. Deep manifold learning for dynamic mr imaging. *ArXiv*, abs/2104.01102:arXiv-2104, 2021.
- [78] Sampurna Biswas, Hemant K Aggarwal, and Mathews Jacob. Dynamic mri using model-based deep learning and storm priors: Modl-storm. *Magnetic Resonance in Medicine*, 82(1):485–494, 2019.
- [79] Tong Zhang, Wenming Zheng, Zhen Cui, and Chaolong Li. Deep manifold-to-manifold transforming network. In *2018 25th IEEE International Conference on Image Processing (ICIP)*, pages 4098–4102, 2018.
- [80] Zhiwu Huang, Ruiping Wang, Xianqiu Li, Wenxian Liu, Shiguang Shan, Luc Van Gool, and Xilin Chen. Geometry-aware similarity learning on spd manifolds for visual recognition. *IEEE Transactions on Circuits and Systems for Video Technology*, 28(10):2513–2523, 2018.
- [81] L. Ambrosio, Italien, and Scuola Normale Superiore). A survey on monge’s optimal transport problem. 2009.
- [82] Dai Shi, Junbin Gao, Xia Hong, S. T. Boris Choy, and Zhiyong Wang. Coupling matrix manifolds assisted optimization for optimal transport problems. *Machine Learning*, 110(3):533–558, 2021.
- [83] B. K. Abid and R. M. Gower. Greedy stochastic algorithms for entropy-regularized optimal transport problems. 2018.
- [84] Arnaud Dessein, Nicolas Papadakis, and Jean Luc Rouas. Regularized optimal transport and the rot mover’s distance. *Journal of Machine Learning Research*, 19, 2016.
- [85] B. Mishra, Ntvs Dev, H. Kasai, and P. Jawanpuria. Manifold optimization for optimal transport. 2021.
- [86] Bamdev Mishra, N T V Satyadev, Hiroyuki Kasai, and Pratik Jawanpuria. Manifold optimization for non-linear optimal transport problems. 2021.
- [87] Viacheslav Borovitskiy, Alexander Terenin, Peter Mostowsky, and Marc Deisenroth (he/him). Matérn gaussian processes on riemannian manifolds. In *Advances in Neural Information Processing Systems*, volume 33, pages 12426–12437, 2020.

- [88] Noémie Jaquier, Viacheslav Borovitskiy, Andrei Smolensky, Alexander Terenin, Tamim Asfour, and Leonel Dario Rozo. Geometry-aware bayesian optimization in robotics using riemannian matérn kernels. In *CoRL*, 2021.
- [89] Arslan Chaudhry, Naeemullah Khan, Puneet Dokania, and Philip Torr. Continual learning in low-rank orthogonal subspaces. *Advances in Neural Information Processing Systems*, 33:9900–9911, 2020.
- [90] Guanxiong Zeng, Yang Chen, Bo Cui, and Shan Yu. Continual learning of context-dependent processing in neural networks. *Nature Machine Intelligence*, 1(8):364–372, 2019.
- [91] Nicolas Boumal, Bamdev Mishra, Pierre Antoine Absil, and Rodolphe J Sepulchre. Manopt, a matlab toolbox for optimization on manifolds. *The Journal of Machine Learning Research*, 15(1):1455–1459, 2014.
- [92] Niklas Koep and Sebastian Weichwald. Pymanopt: A python toolbox for optimization on manifolds using automatic differentiation. *Journal of Machine Learning Research*, 17:1–5, 2016.
- [93] Mayank Meghwanshi, Pratik Jawanpuria, Anoop Kunchukuttan, Hiroyuki Kasai, and Bamdev Mishra. Mctorch, a manifold optimization library for deep learning. Technical report, arXiv preprint arXiv:1810.01811, 2018.
- [94] Nina Miolane, Nicolas Guigui, Alice Le Brigant, Johan Mathe, Benjamin Hou, Yann Thanwerdas, Stefan Heyder, Olivier Peltre, Niklas Koep, Hadi Zaatiti, et al. Geomstats: A python package for riemannian geometry in machine learning. *Journal of Machine Learning Research*, 21(223):1–9, 2020.
- [95] Max Kochurov, Rasul Karimov, and Sergei Kozlukov. Geoopt: Riemannian optimization in pytorch. *ArXiv*, abs/2005.02819:arXiv–2005, 2020.
- [96] Kühnel and Stefan Sommer. Computational anatomy in theano. In *Graphs in Biomedical Image Analysis, Computational Anatomy and Imaging Genetics*, pages 4098–4102, 2017.
- [97] Line Kühnel, Stefan Sommer, and Alexis Arnaudon. Differential geometry and stochastic dynamics with deep learning numerics. *Applied Mathematics and Computation*, 356:411–437, 2019.
- [98] M. Müller, T. Röder, M. Clausen, B. Eberhardt, B. Krüger, and A. Weber. Documentation mocap database hdm05. Technical Report CG-2007-2, Universität Bonn, June 2007.
- [99] Abhinav Dhall, Roland Goecke, Jyoti Joshi, Karan Sikka, and Tom Gedeon. Emotion recognition in the wild challenge 2014: Baseline, data and protocol. In *Proceedings of the 16th International Conference on Multimodal Interaction*, pages 461–466, 2014.

- [100] Lijun Yin, Xiaozhou Wei, Yi Sun, Jun Wang, and M.J. Rosato. A 3d facial expression database for facial behavior research. In *7th International Conference on Automatic Face and Gesture Recognition (FGR06)*, pages 211–216, 2006.
- [101] Arman Savran, Neşe Alyüz, Hamdi Dibeklioglu, Oya Çeliktutan, Berk Gökberk, Bülent Sankur, and Lale Akarun. Bosphorus database for 3d face analysis. In *European Workshop on Biometrics and Identity Management*, pages 47–56, 2008.
- [102] J Ross Beveridge, P Jonathon Phillips, David S Bolme, Bruce A Draper, Geof H Givens, Yui Man Lui, Mohammad Nayeem Teli, Hao Zhang, W Todd Scruggs, Kevin W Bowyer, et al. The challenge of face recognition from digital point-and-shoot cameras. In *International Conference on Biometrics: Theory, Applications and Systems (BTAS)*, pages 1–8. IEEE, 2013.
- [103] Li Fei-Fei and Pietro Perona. A bayesian hierarchical model for learning natural scene categories. In *Proceedings of the IEEE Conference on Computer Vision and Pattern Recognition (CVPR)*, volume 2, pages 524–531, 2005.
- [104] Li-Jia Li and Li Fei-Fei. What, where and who? classifying events by scene and object recognition. In *Proceedings of the IEEE Conference on Computer Vision and Pattern Recognition (CVPR)*, pages 1–8. IEEE, 2007.
- [105] Jianxiong Xiao, James Hays, Krista A Ehinger, Aude Oliva, and Antonio Torralba. Sun database: Large-scale scene recognition from abbey to zoo. In *2010 IEEE Computer Society Conference on Computer Vision and Pattern Recognition*, pages 3485–3492, 2010.
- [106] Jianxiong Xiao, Krista A Ehinger, James Hays, Antonio Torralba, and Aude Oliva. Sun database: Exploring a large collection of scene categories. *International Journal of Computer Vision*, 119(1):3–22, 2016.
- [107] Mengyi Liu, Shiguang Shan, Ruiping Wang, and Xilin Chen. Learning expressionlets on spatio-temporal manifold for dynamic facial expression recognition. In *Proceedings of the IEEE Conference on Computer Vision and Pattern Recognition (CVPR)*, pages 1749–1756, 2014.
- [108] Catalin Ionescu, Orestis Vantzos, and Cristian Sminchisescu. Matrix backpropagation for deep networks with structured layers. In *Proceedings of the IEEE International Conference on Computer Vision*, pages 2965–2973, 2015.
- [109] Tae-Kyun Kim, Josef Kittler, and Roberto Cipolla. Discriminative learning and recognition of image set classes using canonical correlations. *IEEE Transactions on Pattern Analysis and Machine Intelligence*, 29(6):1005–1018, 2007.
- [110] Zhiwu Huang, Ruiping Wang, Shiguang Shan, and Xilin Chen. Projection metric learning on grassmann manifold with application to video based face recognition. In *Proceedings of the IEEE Conference on Computer Vision and Pattern Recognition (CVPR)*, pages 140–149, 2015.

- [111] Hamit Soyel and Hasan Demirel. Optimal feature selection for 3d facial expression recognition using coarse-to-fine classification. *Turkish Journal of Electrical Engineering and Computer Sciences*, 18(6):1031–1040, 2010.
- [112] Stefano Berretti, Alberto Del Bimbo, Pietro Pala, Boulbaba Ben Amor, and Mohamed Daoudi. A set of selected sift features for 3d facial expression recognition. In *International Conference on Pattern Recognition*, pages 4125–4128. IEEE, 2010.
- [113] Xuan-Phung Huynh, Tien-Duc Tran, and Yong-Guk Kim. Convolutional neural network models for facial expression recognition using bu-3dfe database. In *Information Science and Applications (ICISA) 2016*, pages 441–450. 2016.
- [114] Amal Azazi, Syaheerah Lebai Lutfi, Ibrahim Venkat, and Fernando Fernández-Martínez. Towards a robust affect recognition: Automatic facial expression recognition in 3d faces. *Expert Systems with Applications*, 42(6):3056–3066, 2015.
- [115] Soon-Yong Chun, Chan-Su Lee, and Sang-Heon Lee. Facial expression recognition using extended local binary patterns of 3d curvature. In *Multimedia and Ubiquitous Engineering*, pages 1005–1012. 2013.
- [116] Yiding Wang, Meng Meng, and Qingkai Zhen. Learning encoded facial curvature information for 3d facial emotion recognition. In *2013 7th International Conference on Image and Graphics*, pages 529–532, 2013.
- [117] Nicholas Vretos, Nikos Nikolaidis, and Ioannis Pitas. 3d facial expression recognition using zernike moments on depth images. In *2011 18th IEEE International Conference on Image Processing*, pages 773–776, 2011.
- [118] Jihun Hamm and Daniel D Lee. Extended grassmann kernels for subspace-based learning. In *Advances in Neural Information Processing Systems (NIPS)*, pages 601–608, 2009.
- [119] Omkar M Parkhi, Andrea Vedaldi, and Andrew Zisserman. Deep face recognition. 2015.
- [120] Svetlana Lazebnik, Cordelia Schmid, and Jean Ponce. Beyond bags of features: Spatial pyramid matching for recognizing natural scene categories. In *Proceedings of the IEEE Conference on Computer Vision and Pattern Recognition (CVPR)*, volume 2, pages 2169–2178. IEEE, 2006.
- [121] Mandar Dixit, Nikhil Rasiwasia, and Nuno Vasconcelos. Adapted gaussian models for image classification. In *CVPR*, pages 937–943. IEEE, 2011.
- [122] Roland Kwitt, Nuno Vasconcelos, and Nikhil Rasiwasia. Scene recognition on the semantic manifold. In *European Conference on Computer Vision (ECCV)*, pages 359–372, 2012.

- [123] Hanlin Goh, Nicolas Thome, Matthieu Cord, and Joo-Hwee Lim. Learning deep hierarchical visual feature coding. *IEEE Transactions on Neural Networks and Learning Systems*, 25(12):2212–2225, 2014.
- [124] Jianxin Wu and James M Rehg. Beyond the euclidean distance: Creating effective visual codebooks using the histogram intersection kernel. In *IEEE International Conference on Computer Vision*, pages 630–637, 2009.
- [125] Jeff Donahue, Yangqing Jia, Oriol Vinyals, Judy Hoffman, Ning Zhang, Eric Tzeng, and Trevor Darrell. Decaf: A deep convolutional activation feature for generic visual recognition. In *International Conference on Machine Learning (ICML)*, pages 647–655, 2014.

Table 2: Toolboxes Comparison in Terms of Manifolds and Geometry

Toolboxes	Manifolds	Geometry
Manopt [91]	Euclidean manifold, symmetric matrices, sphere, complex circle, SO (n), <i>Stiefel</i> , <i>Graßmannian</i> , oblique manifold, SPD (n), fixed-rank PSD matrices	Exponential and logarithmic maps, tangent space projector, retraction, vector transport, egrad2rgrad, ehess2rhess, vector, metric, distance, norm
Pymanopt [92]	Same as Manopt	Same as Manopt
McTorch [93]	Stiefel, SPD (n)	Same as Manopt
Geoopt [95]	Euclidean manifold, sphere, <i>Stiefel</i> , Poincaré ball	Same as Manopt
Geomstats [94]	Euclidean manifold, Minkowski and hyperbolic space, sphere, SO (n), SE (n), GL (n), <i>Stiefel</i> , <i>Graßmannian</i> , SPD (n), discretized curves, Landmarks	Exponential and logarithmic maps, parallel transport, inner product, distance, norm, Levi-Civita connection, geodesics, invariant metrics
TheanoGeometry [96]	Sphere, ellipsoid, SPD (n), Landmarks, GL (n), SO (n), SE (n)	Inner product, exponential and logarithmic maps, parallel transport, Christoffel symbols, Riemann, Ricci and scalar curvature, geodesics, Fréchet mean

Table 3: Datasets for Different Visual Tasks

Vision Task	Dataset	Total Samples	Categories	Image Size
Character Recognition	MNIST[98]	70000	10	32×32
Emotion Recognition	AFEW [99]	1345	7	400×400
	NABU3DFE [100]	2500	6	NA
	Bosphorus dataset [101]	4666	6	NA
Action Recognition	HDM05 [98]	18000	130	93×93
Face Verification	PaSC [102]	12529	NA	401×401
Scene Recognition	Scene15 [103]	NA	15	300×250
	Eight sports event categories[104]	NA	8	NA
	SUN [105, 106]	899	NA	NA

Table 4: Comparison Results of Character Recognition

Dataset	Method	Accuracy
MNIST [98]	uRNN [14]	97.6%
	full-capacity uRNN [69]	96.9%
	expRNN [13]	98.7%
	soRNN [72]	97.3%
	ORNN [73]	97.2%
	GORU [74]	98.9%

Table 5: Comparison Results of Emotion Recognition

Dataset	Method	Accuracy
AFEW [99]	STM-ExpLet [107]	31.73%
	RSR-SPDML [32]	30.12%
	DeepO2P [108]	28.54%
	DCC [109]	25.78%
	GDA [56]	29.11%
	GGDA [56]	29.45%
	PML [110]	28.98%
	SPDNet [50]	34.23%
BU-3DFE [100]	GrNet [51]	34.23%
	Tree-PNN [111]	93.23%
	Berretti et al. [112]	77.53%
	Huynh et al. [113]	92.73%
	Azazi et al. [114]	85.71%
Bosphorus [101]	Hariri et al. [59]	93.50%
	CSLBP [115]	76.98 %
	CLBP [116]	76.56%
	ZernikeMoments [117]	60.53%
	Azazi et al. [114]	84.10%
Hariri et al. [59]	90.01%	

Table 6: Comparison Results of Action Recognition

Dataset	Method	Accuracy
HDM05 [98]	RSR-SPDML [32]	48.01%
	DCC [109]	41.74%
	GDA [56]	46.25%
	GGDA [118]	46.87%
	PML [110]	47.25%
	SPDNet [50]	61.45%
	GrNet [51]	59.23%

Table 7: Comparison Results of Face Recognition

Method	Accuracy	
	PaSC1 [102]	PaSC2 [102]
VGGDeepFace [119]	78.82%	68.24%
DeepO2P [108]	68.76%	60.14%
DCC [109]	75.83%	67.04%
GDA [56]	71.38%	67.49%
GGDA [118]	66.71%	68.41%
PML [110]	73.45%	68.32%
SPDNet [50]	80.12%	72.83%
GrNet [51]	80.52%	72.76%

Table 8: Comparison Results of Scene Recognition

Dataset	Method	Accuracy
Scene15 [103]	Lazebnik et al. [120]	81.2%
	Dixit et al. [121]	82.3%
	Kwitt et al. [122]	85.4%
	Goh et al. [123]	85.4%
	SRMR [60]	86.9%
Eight sports event categories[104]	Li et al. [104]	73.4%
	Kwitt et al. [122]	83.0%
	Wu and Rehg [124]	84.3%
	SRMR [60]	86.1%
SUN [105]	Xiao et al. [105]	27.2%
	Kwitt et al. [122]	28.9%
	Donahue et al. [125]	30.14%
	SRMR [60]	30.3%